PFC/RR-84-5

DOE/ET/51013-120
UC20G

LINEAR THEORY OF LOWER HYBRID HEATING

Paul Bonoli

Plasma Fusion Center
Massachusetts Institute of Technology
Cambridge, MA 02139

March 27, 1984

This work was supported by the U.S. Department of Energy Contract No. DE-AC02-78ET51013. Reproduction, translation, publication, use and disposal, in whole or in part by or for the United States government is permitted.

LINEAR THEORY OF LOWER HYBRID HEATING

Paul Bonoli

Massachusetts Institute of Technology
Cambridge, Massachusetts 02139

ABSTRACT

The linear theory of wave propagation in the lower hybrid range of frequencies is presented. The topics of accessibility, linear and quasi-linear theories of electron Landau damping, and the linear theory of ion Landau damping are covered. The theory of wave propagation is extended to include the effect of toroidal geometry. A simulation model incorporating these theories is described and numerical results obtained with the model are given.

I. INTRODUCTION

The availability of megawatt microwave sources in the lower hybrid range of frequencies and the use of waveguides external to the vacuum vessel make plasma heating using lower hybrid waves extremely attractive. The original proposals for the use of this method were by Parker and Hooke in 1971 [1] and an extensive review of the linear and nonlinear theory of plasma heating in the lower hybrid range of frequencies was given by Bers in 1978 [1]. In this paper only topics related to the linear theory of wave propagation, linear and quasilinear theory of electron Landau absorption, and the linear theory of ion Landau absorption will be discussed. Important work related to the linear and nonlinear theory of waveguide coupling, the nonlinear theory of parametric processes and the theory of lower hybrid wave scattering from density fluctuations will not be discussed.

The outline of this paper is as follows. In Sec. II the linear theory of wave propagation in slab geometry is presented. The topics of accessibility, linear and quasilinear theory of electron heating, and linear theory of ion heating will be covered. In Sec. III the problem of wave propagation in toroidal geometry will be treated utilizing the technique of geometrical optics and ray tracing. In Sec. IV numerical results of the toroidal ray tracing will be presented for parameters relevant to the Alcator C and Versator II lower hybrid heating experiments. In Sec. V a brief discussion will be given of a simulation model which incorporates a radial transport code, toroidal ray tracing code, and one dimensional Fokker Planck calculation. Numerical results of the model will be given for the Alcator C lower hybrid heating experiment.

II. LINEAR WAVE PROPAGATION AND ABSORPTION IN SLAB GEOMETRY

A. Cold Plasma Electromagnetic Dispersion Relation

The lower hybrid range of frequencies ω satisfies $\Omega_{ce}^2 >> \omega^2 >> \Omega_{ci}^2$, where $\Omega_{c\alpha} = eB_o/m_\alpha$ and $\Omega_{ce}(\Omega_{ci})$ is the electron (ion) gyrofrequency. For typical tokamak magnetic field strengths $B_o = (1.5\ T\text{-}10T)$ this range is roughly $\omega/2\pi = (0.5\text{-}5.0)$ Ghz with $\omega^2 \sim \Omega_{ce}\Omega_{ci}$. The wave propagation is described by a dispersion relation which can be derived as follows [2]. Consider a plasma with density gradient in the x direction direction N(x), a uniform magnetic field in the z direction $\underline{B}_o = \underline{e}_z B_o$, unperturbed electric field $\underline{E}_o = 0$, and unperturbed electron and ion fluid velocities $\underline{v}_{eo} = 0$ and $\underline{v}_{io} = 0$. The perturbed electric field $\underline{E}$, magnetic field $\underline{B}$, and current density $\underline{J}$ are then described by Maxwell's equations,

$$\underline{\nabla} \times \underline{B} = \mu_o \varepsilon_o \frac{\partial}{\partial t} \underline{E} + \mu_o \underline{J} \quad , \tag{1}$$

$$\underline{\nabla} \times \underline{E} = - \frac{\partial}{\partial t} \underline{B} \quad . \tag{2}$$

Assuming that the wave fields vary as $\exp[i(\underline{k}\cdot\underline{x} - \omega t)]$ and $|\underline{k}| >> |\partial/\partial \underline{x}|$ (WKB approximation), Eqs. (1) and (2) can be Fourier analyzed in space and time to yield the wave equation,

$$-\underline{k} \times \underline{k} \times \underline{E} = (\omega/c)^2 \underline{E} + i\omega\mu_o \underline{J} \quad . \tag{3}$$

Note that no assumption has been made about the electric field polarization, i.e. $\underline{E} = \underline{e}_x E_x + \underline{e}_y E_y + \underline{e}_z E_z$. In the limit of a "cold" plasma [$T_e = 0$ and $T_i = 0$, where $T_e(T_i)$ is the electron (ion) temperature], the perturbed

current density $\underline{J}$ can be expressed as $\underline{J} = Ne(\underline{v}_i - \underline{v}_e)$. The perturbed electron (ion) fluid velocities $\underline{v}_e(\underline{v}_i)$ can be expressed in terms of $\underline{E}$ using the two-fluid momentum equations,

$$m_e \frac{\partial}{\partial t} \underline{v}_e = - e(\underline{E} + \underline{v}_e \times \underline{B}_o) \quad , \tag{4}$$

$$m_i \frac{\partial}{\partial t} \underline{v}_i = e(\underline{E} + \underline{v}_i \times \underline{B}_o) \quad . \tag{5}$$

Assuming that $\underline{v}_e$, $\underline{v}_i$ vary as $\exp[i(\underline{k}\cdot\underline{x}-\omega t)]$ one then uses Eqs. (3), (4), and (5) to obtain,

$$\underline{k} \times \underline{k} \times \underline{E} + (\omega/c)^2 \, \underline{\underline{\varepsilon}} \cdot \underline{E} = 0 \quad , \tag{6a}$$

$$\underline{\underline{\varepsilon}} = \begin{bmatrix} \varepsilon_\perp & -i\varepsilon_{xy} & 0 \\ i\varepsilon_{xy} & \varepsilon_\perp & 0 \\ 0 & 0 & \varepsilon_\parallel \end{bmatrix} \quad . \tag{6b}$$

$\underline{\underline{\varepsilon}}$ is the familiar cold plasma dielectric tensor of Stix [2] whose elements are evaluated in the limit $\Omega_{ce}^2 >> \omega^2 >> \Omega_{ci}^2$ and are given by,

$$\varepsilon_\perp = 1 + (\omega_{pe}/\Omega_{ce})^2 - (\omega_{pi}/\omega)^2 \quad , \tag{7a}$$

$$\varepsilon_\parallel = 1 - (\omega_{pe}/\omega)^2 - (\omega_{pi}/\omega)^2 \quad , \tag{7b}$$

$$\varepsilon_{xy} = \omega_{pe}^2/(\omega\Omega_{ce}) \quad . \tag{7c}$$

Here $\omega_{p\alpha} = (Ne^2/\varepsilon_o m_\alpha)^{1/2}$ and ω_{pe} (ω_{pi}) is the electron (ion) plasma frequency. Equation (6) may be written in a more compact form by first defining

$\underline{D} = \underline{k} \times \underline{k} \times \underline{1} + (\omega/c)^2 \underline{\varepsilon}$. Then,

$$\underline{D} \cdot \underline{E} = 0 \quad . \tag{8}$$

The solution to the system of equations (8) will be nontrivial provided the determinant of the system vanishes, $D_o \equiv \det \underline{D} = 0$. This condition yields the cold plasma, electromagnetic, lower hybrid dispersion relation,

$$D_o(\underline{x},\underline{k},\omega) = P_4 \, n_\perp^4 + P_2 \, n_\perp^2 + P_o = 0 \quad , \tag{9}$$

$$P_o = \varepsilon_\parallel \left[(n_\parallel^2 - \varepsilon_\perp)^2 - \varepsilon_{xy}^2 \right] \quad ,$$

$$P_2 = (\varepsilon_\perp + \varepsilon_\parallel)(n_\parallel^2 - \varepsilon_\perp) + \varepsilon_{xy}^2 \quad ,$$

$$P_4 = \varepsilon_\perp \quad ,$$

where $n_\parallel = k_\parallel c/\omega$, $n_\perp = k_\perp c/\omega$, $k_\parallel = \underline{k} \cdot \underline{B}/|\underline{B}|$, and $\underline{k}_\perp = \underline{k} - k_\parallel \underline{B}/|\underline{B}|$. Equation (9) indicates two modes of wave polarization in terms of $n_\perp^2$,

$$n_\perp^2 = \frac{1}{2P_4} \left(- P_2 \pm \Delta^{1/2} \right) \quad , \tag{10}$$

$$\Delta = (P_2)^2 - 4P_o P_4 \quad .$$

In the lower hybrid frequency range $|\varepsilon_\parallel| \gg \varepsilon_\perp, \varepsilon_{xy}$, so that typically $P_o > 0$ and $P_2 < 0$. The "slow" wave branch (small $\omega/k_\perp$) of the dispersion relation then corresponds to the positive sign in (10) and the "fast" wave branch (large $\omega/k_\perp$) corresponds to the minus sign in (10). The slow wave branch will have a cold plasma resonance ($n_\perp \to \infty$) for $P_4 = \varepsilon_\perp = 0$, thus defining the lower hybrid frequency $\omega_{\ell h}$ such that [see Eq. (7a)],

$\omega_{\ell h} \equiv \omega = \omega_{pi}/(1+\omega_{pe}^2/\Omega_{ce}^2)^{1/2}$. It is this slow wave branch of the dispersion relation one typically associates with the lower hybrid wave.

Figures 1(a) - 1(c) show plots of $n_\perp^2$ versus density N(x) for three different values of $n_\parallel$ [using Eq.(10)]. It is important to note that there exists a critical value of the parallel index of refraction $n_\parallel \equiv n_a$ for which a wave which is launched at the slow wave cutoff ($n_\perp = 0$ denoted by N_s in Fig. 1) with $n_\parallel \geq n_a$, will propagate to its resonance ($n_\perp \to \infty$ denoted by N_{LH} in Fig. 1) without converting to the fast wave. This situation ($n_\parallel \geq n_a$) is depicted in Figs. 1(b) and 1(c). If $n_\parallel < n_a$ [see Fig. 1(a)] then a wave launched at the slow wave cutoff N_s will mode convert to the fast wave at a density denoted by N_{T1} in Fig. 1, thus propagating out to the fast wave cutoff ($n_\perp = 0$ denoted by N_F in Fig. 1). The fast wave will then reflect and mode convert back to the slow wave at N_{T1}, this process being repeated ad infinitum. A detailed analysis [2,3,4,5,6] of Eq.(10) gives the lowest value of $n_\parallel = n_a$ for which the lower hybrid or slow wave will be able to propagate from its cutoff to the maximum plasma density in the presence of a density gradient without mode converting to the inaccessible fast wave ($\Delta \geq 0$). Two cases can be distinguished and they comprise the accessibility condition [2,3,4,5,6],

(i) If $\Omega^2 < 1$ and $\dfrac{\omega_{pio}^2}{\omega^2} > \Omega^2/(1-\Omega^2)$, then

$$n_a = (1-\Omega^2)^{-1/2} . \tag{11a}$$

(ii) If $\Omega^2 > 1$ or $\Omega^2 < 1$ and $\dfrac{\omega_{pio}^2}{\omega^2} < \Omega^2/(1-\Omega^2)$, then

$$n_a = \frac{\omega_{peo}}{\Omega_{ceo}} + \varepsilon_{\perp o}^{1/2} . \tag{11b}$$

Here $\Omega^2 = \omega^2/(\Omega_{ce}\Omega_{ci})$ and the subscript o denotes evaluation at the maximum plasma density.

B. Cold Plasma Electrostatic Dispersion Relation

If one considers propagation of the slow wave at densities much greater than those corresponding to the cutoff densities N_S and N_F, then the lower hybrid wave polarization is essentially electrostatic ($kc/\omega \gg 1$). In this case the dispersion relation (9) reduces to the familiar result,

$$D_o(\underline{x}, \underline{k}, \omega) = \varepsilon_\perp k_\perp^2 + \varepsilon_\parallel k_\parallel^2 = 0. \tag{12}$$

The idea [7] of a lower hybrid wave propagating along a well-defined resonance cone can be motivated using Eq. (12) [8]. Consider a point source which excites an electrostatic disturbance in a plasma with frequency and wavenumber $(\omega, k_\parallel)$, satisfying the dispersion relation (12). For simplicity take $\underline{k} = \underline{e}_x k_\perp + \underline{e}_z k_\parallel$ and $\underline{E} = -\underline{\nabla}\phi$, where $\phi \sim \exp[i(k_\perp x + k_z z - \omega t)]$. Then the Fourier transforms in (12) may be inverted to give,

$$\frac{\partial^2 \phi}{\partial x^2} = -\left(\frac{\varepsilon_\parallel}{\varepsilon_\perp}\right) \frac{\partial^2 \phi}{\partial z^2} \quad . \tag{13}$$

This equation is identical to the familiar wave equation,

$$\frac{\partial^2 \psi}{\partial t^2} = C^2 \frac{\partial^2 \psi}{\partial z^2} \quad , \tag{14}$$

if x is replaced by t and $-(\varepsilon_\parallel/\varepsilon_\perp)$ is replaced by C^2. The solutions of Eq. (14) propagate along characteristics $z \pm ct$. In analogous fashion, the solutions of (13) propagate along characteristics $z \pm (-\varepsilon_\parallel/\varepsilon_\perp)^{1/2} x$. These are the resonance cones, representing the propagation path of a singular electrostatic disturbance excited by a point source and obeying the lower hybrid dispersion relation. In reality a lower hybrid wave launching structure on a tokamak will have a finite poloidal extent. In this case

the antenna can be modelled by many point sources and cone theory can be used to calculate the electric field excited by such a structure [9,10] (this field resulting from the superposition of the resonance cone patterns evolving from each point source). Resonance cones were first observed experimentally by Fisher and Gould [11] and lower hybrid resonance cones were first observed by Briggs and Parker [12].

C. Warm Plasma Effects

The cold plasma singularity for $n_\perp$ is removed by including finite electron and ion temperature in the analysis of Sec. IIA. An analysis identical to that of Sec. IIA is followed, except that the perturbed current density $\underline{J}$ is expressed in terms of the perturbed electron and ion distribution functions $f_e(\underline{v})$ and $f_i(\underline{v})$, as

$$\underline{J} = Ne \left[\int \underline{v} f_i(\underline{v}) d\underline{v} - \int \underline{v} f_e(\underline{v}) d\underline{v} \right] . \tag{15}$$

The perturbed functions $f_e(\underline{v})$ and $f_i(\underline{v})$ are solved by first linearizing the Vlasov equation for each species about the unperturbed distribution functions f_{eo} and f_{io} [13],

$$\frac{\partial}{\partial t} f_e + \underline{v} \cdot \frac{\partial}{\partial \underline{x}} f_e - \frac{e}{m_e} \underline{v} \times B_o \cdot \frac{\partial}{\partial \underline{v}} f_e =$$

$$\frac{e}{m_e} (\underline{E} + \underline{v} \times \underline{B}) \cdot \frac{\partial}{\partial \underline{v}} f_{eo} , \tag{16a}$$

$$\frac{\partial f_i}{\partial t} + \underline{v} \cdot \frac{\partial}{\partial \underline{x}} f_i + \frac{e}{m_i} \underline{v} \times \underline{B}_o \cdot \frac{\partial}{\partial \underline{v}} f_i =$$

$$- \frac{e}{m_i} (\underline{E} + \underline{v} \times \underline{B}) \cdot \frac{\partial}{\partial \underline{v}} f_{io} . \tag{16b}$$

The equilibrium distribution functions are assumed to have the form

$$f_{eo} = \frac{1}{(2\pi)^{3/2}} \frac{1}{v_e^3} \exp \left[- \frac{v_\perp^2 + v_\parallel^2}{2v_e^2} \right] ,$$

$$f_{io} = \frac{1}{(2\pi)^{3/2}} \frac{1}{v_i^3} \exp\left[- \frac{v_\perp^2 + v_\parallel^2}{2v_i^2} \right] ,$$

where $v_e = (T_e/m_e)^{1/2}$ is the electron thermal speed, $v_i = (T_i/m_i)^{1/2}$ is the ion thermal speed, and $v_\perp$ ($v_\parallel$) denotes the magnitude of velocity perpendicular (parallel) to the applied magnetic field $\underline{B}_o$. Using the method of characteristics, (or integrating along the orbits of the particles in the unperturbed fields) [2,13], the perturbed distribution functions can be solved from Eqs. (16a) and (16b). Using this result in Eqs. (15) and (3) one then obtains the following result for the thermal correction to the lower hybrid dispersion relation [2,14,15],

$$D_R(\underline{x}, \underline{k}, \omega) = P_6 n_\perp^6 + P_4 n_\perp^4 + P_2 n_\perp^2 + P_o = 0, \tag{17}$$

$$P_6 = - \left[3 \frac{\omega_{pi}^2}{\omega^2} \frac{v_i^2}{c^2} + \frac{3}{4} \frac{\omega_{pe}^2}{\Omega_{ce}^2} \frac{\omega^2}{\Omega_{ce}^2} \frac{v_e^2}{c^2} \right] ,$$

where P_o, P_2, and P_4 were defined earlier. In deriving Eq. (17) it has been assumed that $(k_\perp \rho_e)^2 << 1$ and $\Omega_{ci}^2 >> \omega^2 >> \Omega_{ce}^2$. Here $\rho_e = v_e/\Omega_{ce}$ is the electron Larmor radius and the ions are taken to be essentially unmagnetized (straight line orbits).

The $n_\perp^6$ term is the thermal wave branch of the dispersion relation (ion plasma wave). This branch is shown in Figs. 2(a) - 2(c) for three different values of n_a. The density N_{MC}, at which an incoming lower hybrid wave is mode converted to an ion plasma wave is found by taking the electrostatic limit of Eq. (17) ($kc/\omega >> 1$),

$$\delta k_{\perp}^4 + \varepsilon_{\perp} k_{\perp}^2 + k_{\parallel}^2 \varepsilon_{\parallel} = 0 \quad , \tag{18}$$

$$\delta = (c/\omega)^2 \, P_6 \quad .$$

Notice that the electromagnetic fast wave branch has been eliminated. The density at which the lower hybrid and ion plasma wave branches coalesce [i.e., $\varepsilon_{\perp}^2 = 4\delta k_{\parallel}^2 \varepsilon_{\parallel}$] is then given by,

$$\omega_{LH}^2(x_{Mc}) = \omega^2 \left\{ 1 + 2\sqrt{3} n_{\parallel} \frac{v_e}{c} \left(\frac{T_i}{T_e}\right)^{1/2} \left[1 + \frac{1}{4} \frac{T_e}{T_i} \Omega^4 \right]^{1/2} \right\}^{-1} \quad . \tag{19}$$

Equation (19) can be combined with the fact that at the point of ion mode conversion $k_{\perp}^2 = -\varepsilon_{\perp}/(2\delta)$, to yield a useful expression for the ratio of perpendicular phase velocity to ion thermal speed [15],

$$\left(\frac{\omega}{\sqrt{2} k_{\perp} v_i} \right)_{Mc} \simeq \frac{4.4}{n_{\parallel}^{1/2}} \, \frac{1}{[T_i(\text{keV})]^{1/4}} \quad .$$

Here it has been assumed that $[1 + \frac{1}{4} \frac{T_e}{T_i} \Omega^4]^{1/2} \sim 1$. For parameters typical of the Alcator C lower hybrid heating experiment $n_{\parallel} \sim 3$ and $T_i \sim 1$ keV, so that $(\omega/\sqrt{2} k_{\perp} v_i)_{MC} \simeq 2.54$. It is worth noting that just as the accessibility of the lower hybrid wave is determined by its axial index of refraction $n_{\parallel}$ (Sec. IIA) so also does $n_{\parallel}$ determine the spatial location of ion mode conversion [see Eq. (19)].

D. Linear Resonant Wave Absorption

In deriving Eq. (17) one also finds resonant imaginary contributions to the dispersion relation due to electrons and ions. These contributions give rise to Landau damping of the lower hybrid wave on plasma ions and electrons and are given by [2,15,16,17],

$$D_I^{(e)} = 2\pi^{1/2} \frac{\omega_{pe}^2}{\omega^2} (n_\perp n_\parallel)^2 I_o(\lambda_e) e^{-\lambda_e} x_{oe}^3 e^{-x_{oe}^2} \tag{20a}$$

$$\lambda_e = (k_\perp v_e/\Omega_{ce})^2 \quad ,$$

$$x_{oe} = \omega/(\sqrt{2} k_\parallel v_e) \quad .$$

$$D_I^{(i)} = \pi^{1/2} n_\perp^2 \frac{\omega_{pi}^2}{\omega^2} \frac{c^2}{v_i^2} \cdot \sum_{n=-\infty}^{\infty} I_n(\lambda_i) e^{-\lambda_i} x_{oi} e^{-x_{ni}^2} \tag{20b}$$

$$\lambda_i = (k_\perp v_i/\Omega_{ci})^2 \quad ,$$

$$x_{oi} = \omega/(\sqrt{2} k_\parallel v_i)$$

$$x_{ni} = (\omega - n\Omega_{ci})/(\sqrt{2} k_\parallel v_i) \quad ,$$

where I_n is the modified Bessel function of order n. The electron contribution can be easily simplified since $\lambda_e \ll 1$ (strongly magnetized electrons). The ion contribution must be evaluated carefully in the large λ_i limit using a Hadamard expansion [15,16.17]. The results are,

$$D_I^{(e)} = 2\pi^{1/2} \frac{\omega_{pe}^2}{\omega^2} (n_\perp n_\parallel)^2 x_{oe}^3 e^{-x_{oe}^2} , \qquad (21a)$$

$$D_I^{(i)} = 2\pi^{1/2} \frac{\omega_{pi}^2}{\omega^2} n_\perp^4 x_{oi}^3 e^{-x_{oi}^2} \left\{ \frac{1}{\pi^{1/2}} \sum_{n=-\infty}^{\infty} \frac{\Omega_{ci}}{\omega} x_{oi} e^{-x_{ni}^2} \right\} . \qquad (21b)$$

The ion damping term consists of a piece which is identical to the electron damping term, except that it is multiplied (or "modulated") by an infinite sum. In the limit where $\Omega_{ci}/(\sqrt{2}k_\parallel v_i)<<1$, the e-folding length of the exponential in the infinite sum of Eq. (21b) is large compared to the distance between adjacent ion-cyclotron surfaces where $x_{ni}=0$ (i.e. $\omega=n\Omega_{ci}$). In this case the infinite sum can be converted to an equivalent spatial integral over many cyclotron harmonics of the plasma. The resulting integral is approximately equal to unity and the ion damping term takes the form of the electron damping and the result is identical to treating the ions as unmagnetized [15,18]

$$D_I^{(i)} = 2\pi^{1/2} \frac{\omega_{pi}^2}{\omega^2} n_\perp^4 x_{oi}^3 e^{-x_{oi}^2} . \qquad (22)$$

However the inequality $\Omega_{ci}/(\sqrt{2}k_\parallel v_i)<<1$ is not usually satisfied in the lower hybrid frequency range. Instead one might attempt some type of numerical evaluation of the infinite sum in (21b) [15,19,20,21]. Alternatively one can adopt the viewpoint that Eq. (22) can be used to evaluate the ion damping so long as a physical mechanism exists which destroys phase correlations over a cyclotron period. In the limit $\omega>>\Omega_{ci}$, phase mixing occurs on time scales much shorter than a cyclotron period Ω_{ci}^{-1}, but after a whole period the exact phase correlations are restored, and no damping is recovered [22].

However a de-correlation mechanism has been proposed by Karney [23,24,25] in the form of stochastic ion heating. Stochastic ion motion could arise in the presence of a lower hybrid wave (with electric field amplitude above a certain threshold) due to the nonlinear interaction of the resonances between the cyclotron motion and the wave motion even for $\omega >> \Omega_{ci}$ [24]. The ions would then be heated since much of the phase space is accessible to a given ion. Furthermore if the lower hybrid wave amplitude is far above the stochasticity threshold, ion Landau damping (Eq. 22) is recovered [25] (because the ion motion is stochastic, the cyclotron harmonic resonance is destroyed since an ion will now forget its phase relative to the wave in a cyclotron period). For the purposes of this paper it will be sufficient to take the electron and ion damping terms to be those given by Eqs. (21a) and (22).

A simple estimate of the critical parallel phase velocity at which electron Landau damping becomes important $x_{oe}^{(c)}$ and the critical perpendicular phase velocity at which ion Landau damping becomes important $x_{oi}^{(c)}$ can be made from Eqs. (21a) and (22). The spatial resonant damping of the wave takes the form,

$$P(x) = P_o \exp\left[2 \int_o^x k_I(x)dx \right] ,$$

where $P(x)$ is the power in the wave, $P_o = P(x=0)$, and k_I is the imaginary part of $k_\perp = k_{\perp R} + ik_I$. An expression for k_I is found in the usual way by expanding $D_o(\underline{x}, \underline{k}, \omega) = D_R(\underline{x}, \underline{k}, \omega) + iD_I^{(e)}(\underline{x}, \underline{k}, \omega) + iD_I^{(i)}(\underline{x}, \underline{k}, \omega) = 0$ about $k_{\perp R}$ in the limit of weak damping $k_I << k_{\perp R}$. The result is

$$k_I = - \frac{D_I^{(e)}(\underline{x},\underline{k}_R,\omega) + D_I^{(i)}(\underline{x},\underline{k}_R,\omega)}{(\partial D_R/\partial k_\perp)_{\underline{k}=\underline{k}_R}} \quad . \tag{23}$$

The damping for electrons and ions becomes important when $|2k_I \Delta x_D| \sim 1$, where Δx_D is a typical scale length of the damping. The electron contribution to k_I is then evaluated using the cold plasma electrostatic limit of Eq. (17) in Eq. (23), along with (21a). The condition for significant damping then becomes [1,3,5,26],

$$4\pi^{3/2}(m_i/m_e)^{1/2} \frac{(\omega/2\pi)}{c} n_{||} x_{oe}^3 e^{-x_{oe}^2} \Delta x_D \sim 1. \tag{24}$$

Assuming typical Alcator C parameters with $\omega/2\pi = 4.6$ GHz, $n_{||} \sim 2$, and $\Delta x_D \sim 1$ cm, (24) then yields $x_{oe} \equiv x_{oe}^{(c)} \simeq 2.8 - 3.0$. A similar analysis of the ion contribution to k_I using Eq. (22) yields $x_{oi} \equiv x_{oi}^{(c)} \simeq 2.8 - 3.0$. These values of $x_{oi}^{(c)}$ and $x_{oe}^{(c)}$ are the linear limits of ion and electron Landau damping. Recalling Eq. (19) it can be seen that at the point of ion mode conversion the perpendicular phase velocity should be small enough to satisfy $x_{oi} \lesssim x_{oi}^{(c)}$ and thus significant ion Landau damping would be expected at this point. Just as $n_{||}$ played an important role in determining accessibility and ion wave absorption, it can also be seen that it determines electron Landau damping $x_{oe} \lesssim x_{oe}^{(c)}$.

E. Linear Nonresonant Absorption

In the low temperature region near the edge of a tokamak plasma, the electron-ion Coulomb collision frequency $\nu_{ei} \propto N/T_e^{3/2}$ can become important relative to the wave frequency ω. This gives rise to a nonresonant contribution to the imaginary part of the dispersion relation proportional to (ν_{ei}/ω). This contribution can be evaluated by repeating the analysis of Sec. IIA with a collision term included in the electron momentum equation (4),

$$m_e \frac{\partial \underline{v}_e}{\partial t} = - e \left(\underline{E} + \underline{v}_e \times \underline{B}_o \right) + m_e (\underline{v}_i - \underline{v}_e) \nu_{ei} \quad . \tag{25}$$

The use of the cold plasma equations is justified here since the collisional damping is expected to be most important in the low temperature region. The result for the imaginary contribution is [8],

$$D_I^{(\ell)}(\underline{x},\underline{k},\omega) = \frac{\nu_{ei}}{\omega} \left[\frac{\omega_{pe}^2}{\Omega_{ce}^2} n_\perp^2 + \frac{\omega_{pe}^2}{\omega^2} n_\parallel^2 \right] n_\perp^2 \quad . \tag{26}$$

F. Quasilinear Electron Landau Damping

A better estimate of the electron Landau damping can be made by the use of quasilinear theory [27]. It is no longer assumed that the steady state distribution function is a Maxwellian but rather evolves according to the one dimensional Fokker Planck equation [28],

$$\frac{\partial F}{\partial t} = \frac{\partial}{\partial v_\parallel} D_{q\ell}(v_\parallel) \frac{\partial F}{\partial v_\parallel} + \frac{\partial}{\partial v_\parallel} \nu(v_\parallel) \left[v_\parallel F + v_e^2 \frac{\partial F}{\partial v_\parallel} \right] , \tag{27}$$

$$\nu(v_\parallel) = \nu_o (v_e / v_\parallel)^3$$

$$\nu_o = \log \Lambda \; \omega_{pe}^4 / (2\pi N v_e^3)(2 + Z_e)/2 \quad .$$

Log Λ is the Coulomb logarithm, Z_e is the effective charge state of the plasma, $\nu(v_\parallel)$ is an effective collision frequency, $D_{q\ell}(v_\parallel)$ is a quasilinear diffusion coefficient due to Landau damping [30] and proportional to the power spectrum of lower hybrid waves. In deriving (27) a form for $f_{eo} \alpha \exp(-v_\perp^2/v_e^2) F(v_\parallel)$ has been assumed and the limit $v_\parallel^2 >> v_e^2$ has been taken (high velocity equation).

The resulting distribution function is then a result of the competition between the quasilinear "flattening" or plateau formation due to the parallel velocity diffusion of electrons ($D_{q\ell}$) and the effect of electron collisions (which tend to restore F to a Maxwellian). A quantitative assessment of this effect can be obtained by integrating the steady state equation (27) $\partial F/\partial t = 0$ to obtain,

$$\frac{\partial F(x_{oe})}{\partial x_{oe}} = - \frac{2x_{oe}F(x_{oe})}{1+2\sqrt{2}Dx_{oe}^3} \quad , \quad D = D_{q\ell}/(\nu_o v_e^2) \quad , \tag{28}$$

where $v_{||}$ has been conveniently normalized to $x_{oe} = v_{||}/(\sqrt{2}v_e)$. Note that D is a ratio of the quasilinear diffusion to collisional diffusion ($\nu_o v_e^2$). Integrating (28) yields,

$$F(x_{oe}) = F_o \exp\left[- \int_{x_{oe}} \frac{2x_{oe}dx_{oe}}{1+2\sqrt{2}Dx_{oe}^3} \right] \quad . \tag{29}$$

From Sec. IIE one can guess that the region of power $D \neq 0$ of the lower hybrid wave should extend down to phase velocities $x_{oe} \lesssim x_{oe}^{(c)} \sim 3$ if Landau damping is to occur. At this point the denominator in the exponent of (29) will be large for values of $D \gtrsim 1/2$. There a plateau will then form on F with a value $F[x_{oe}^{(c)}] \simeq F_o \exp\left[-(x_{oe}^{(c)})^2 \right]$, where $F(x_{oe})$ is assumed to be Maxwellian in the part of velocity space below the region of power $x_{oe} < x_{oe}^{(c)}$. The slope of F near the critical velocity for Landau damping is then given by (28) as,

$$\left.\frac{\partial F}{\partial x_{oe}}\right|_{x_{oe}^{(c)}} \simeq - \left. \frac{2x_{oe}F_o e^{-x_{oe}^2}}{1+\sqrt{2}\,x_{oe}^3} \right|_{x_{oe}^{(c)}} \quad , \tag{30}$$

where $D \sim 1/2$ has been used. A crude estimate of the new quasilinear limit for $x_{oe}^{(c)}$ can then be made by substituting Eq. (30) into Eq. (24) in place of $-2x_{oe}\exp(-x_{oe}^2) \sim \partial F/\partial x_{oe}$. The result is,

$$4\pi^{3/2}(m_i/m_e)^{1/2}\ \frac{\omega/2\pi}{c}\ n_{\parallel}\Delta x_D\ \frac{x_{oe}^3\ e^{-x_{oe}^2}}{1+\sqrt{2}x_{oe}^3} \sim 1 \quad . \tag{31}$$

Again assuming typical Alcator C parameters $\omega/2\pi = 4.6$ GHz, $n_{\parallel} \sim 2.0$, and $\Delta x_D \sim 1$ cm, one obtains $x_{oe} \equiv x_{oe}^{(c)} \simeq 2.3$ [5,26,27,31]. Thus the quasilinear estimate for $x_{oe}^{(c)}$ is considerably smaller than the linear estimate of $x_{oe}^{(c)} \gtrsim 3.0$, so that a lower hybrid wave with fixed $(\omega, k_{\parallel})$ should penetrate to a higher temperature region of the plasma in the quasilinear limit, before being absorbed via electron Landau damping.

III. Linear Wave Propagation and Absorption in Toroidal Geometry

It can be seen from the discussion of Sec. II that the accessibility and absorption of the lower hybrid wave depend sensitively on the parallel index of refraction $n_{||}$. In the slab model of wave propagation in a one dimensionally inhomogeneous plasma, the $k_{||} \equiv k_z$ (or $n_{||}$) of the incident lower hybrid wave would be fixed by the axial dimensions of the antenna launching structures (in this case a set of waveguides) or "Grill" [29]. The dispersion relation $D_o(x, k_x, k_z, \omega) = 0$ is all that is needed to prescribe $k_x(x)$.

The results of the slab theory can be extended to a cylindrical (r,θ,z) geometry by considering a plasma with axial (z) and poloidal (θ) symmetry, a radially varying density $N(r)$, and magnetic field $\underline{B} = \underline{e}_z B_o + \underline{e}_\theta B_\theta(r)$, with constant B_o and $B_\theta << B_o$. The perturbed fields are assumed to vary as $\exp[i(m\theta + k_z z - \omega t)]$ with m and k_z fixed by the launching structure (note that m and k_z are constant owing to the poloidal and axial symmetry of the plasma). Taking $\underline{k} = \underline{e}_r k_r + \underline{e}_\theta (m/r) + \underline{e}_z k_z$, then $k_{||} = \underline{k}\cdot\underline{B}/|\underline{B}|$ is given by,

$$k_{||} = \left[(m/r)B_\theta(r) + k_z B_o\right]/B \quad ,$$

and $k_{||}$ is approximately constant since $B_\theta(r) \sim r$ near $r = 0$ and $m \simeq 0$ at the waveguide is fixed. Again the dispersion relation $D_o(r,k_r,k_z,\omega) = 0$ prescribes $k_r(r)$ completely.

In an axially symmetric tokamak geometry (r,θ,ϕ) the toroidal magnetic field is $B_\phi(r,\theta) \simeq B_o/[1 + (r/R_o)\cos\theta]$ and the equilibrium is two dimensionally inhomogeneous in (r,θ). Here ϕ is the toroidal angle, R_o is the torus major radius, and a is the torus minor radius. In addition, the concentric flux surfaces of constant density and constant radius in the cylindrical geometry become shifted, nonconcentric flux surfaces in the tokamak geometry [32].

The degenerate ($r \to 0$) flux surface called the magnetic axis is shifted from the geometrical center of the tokamak chamber by an amount which is of the order of $\varepsilon \equiv a/R_o$ (the inverse aspect ratio of the torus) [32]. The perturbed field quantities now vary as $\exp[i(n\phi-\omega t)]$, where n is the toroidal mode number, $\underline{k} = \underline{e}_r k_r + \underline{e}_\theta (m/r) + \underline{e}_\phi (n/R)$, and $R = R_o + r\cos\theta$ is the major radial position. The toroidal mode number n is constant owing to the axial symmetry of the tokamak, whereas the poloidal mode number is no longer a conserved quantity because of the poloidal asymmetry of the equilibrium. There are two interesting consequences of this. First is that the dispersion relation $D_o(r,\theta;\, k_r,m,n,\omega) = 0$ no longer completely prescribes $k_r(r)$. Instead the wave is confined to a path in $(r,\theta;\, k_r,m)$ space. The second consequence is that $k_{||}$ can now change significantly as the wave propagates. Taking $\underline{B} = \underline{e}_r B_r(r,\theta) + \underline{e}_\theta B_\theta(r,\theta) + \underline{e}_\phi B_\phi(r,\theta)$ with $|B_r| << B_\theta << B_\phi$ [32], $k_{||}$ is given by,

$$k_{||} = (k_r B_r + \frac{m}{r} B_\theta + \frac{n}{R} B_\phi)/B \quad .$$

$k_{||}$ changes due to variations in m (toroidal effect) and magnetic shear (B_θ). Thus the accessibility and wave absorption determined by the value of the wave $(\omega, k_{||})$ at the plasma edge will change as the wave propagates to the plasma interior, making global predictions of wave accessibility and absorption impossible.

This situation can be treated by application of the eikonal method [33]. The essence of this method lies in assuming that although an electromagnetic (EM) wave may not be able to be characterized as a plane wave in general, that within each small region of space, the EM wave possesses plane wave properties. That is, within each small region the amplitude and direction of the wave remain nearly constant over the distance of a wavelength.

This satisfied, one then constructs surfaces of constant phase (wave surfaces), where a plane wave surface is simply a plane perpendicular to the direction of propagation. In each region of space one has a direction of propagation of the wave, normal to the wave surface. The propagation of the wave is then described through the concept of a ray - which would just be a curve whose tangents at each point coincide with the direction of propagation of the wave. Clearly this picture of treating the propagation of waves as simply the propagation of rays becomes more and more accurate in the limit of the wavelength $\lambda \to 0$ (i.e., limit of geometrical optics) [33]. One then proceeds to represent field quantities such as the electric field as

$$\underline{E} = \underline{E}_o \exp[iS(\underline{x},t)] \quad , \tag{32}$$

where in the zeroth approximation $\underline{E}_o$ is constant and all the spatial and time changes in $\underline{E}$ are contained in the large, rapidly varying phase factor $S(\underline{x},t)$, which is also known as the eikonal. For each small region of space where the plane wave representation for $\underline{E}$ is valid [i.e., $\underline{E} = E_o \exp(i\underline{k}\cdot\underline{x}-i\omega t)$], the eikonal may be expanded in a Taylor series as,

$$S = S_o + \underline{x} \cdot \frac{\partial S}{\partial \underline{x}} + t \frac{\partial S}{\partial t} \quad .$$

Comparing this with the plane wave representation one sees that

$$\underline{k} = \frac{\partial S}{\partial \underline{x}} = \underline{\nabla} S \quad , \tag{33a}$$

$$\omega = - \frac{\partial S}{\partial t} \quad . \tag{33b}$$

One of the main results of the eikonal method is that Eq. (33a) is the solution of the local dispersion relation $D_o(\underline{x},\underline{k},\omega) = 0$ and that the wave

evolves in $(\underline{x},\underline{k})$ space according to the ray equations of geometrical optics [2,34],

$$\frac{d\underline{x}}{dt} = - \frac{\partial D_o/\partial \underline{k}}{\partial D_o/\partial \omega} \quad , \tag{34a}$$

$$\frac{d\underline{k}}{dt} = + \frac{\partial D_o/\partial \underline{x}}{\partial D_o/\partial \omega} \quad . \tag{34b}$$

The condition that the wavelength λ be much less than a typical plasma scale length is well-satisfied for the lower hybrid wave except near the plasma cutoffs ($n_\perp \to 0$) and turning points ($dk_\perp/dx \gtrsim k_\perp^2$). Following Ref. [35], the ray equations can be written in a particularly simple form in toroidal geometry if one utilizes their Hamiltonian nature. Letting $\underline{x} = (r,\theta,\phi)$ and $\underline{k} = (k_r,m,n)$ the ray equations (34) become [35],

$$\frac{dr}{dt} = - \frac{\partial D_o/\partial k_r}{\partial D_o/\partial \omega} \quad , \tag{35a}$$

$$\frac{d\theta}{dt} = - \frac{\partial D_o/\partial m}{\partial D_o/\partial \omega} \quad , \tag{35b}$$

$$\frac{d\phi}{dt} = - \frac{\partial D_o/\partial n}{\partial D_o/\partial \omega} \quad , \tag{35c}$$

$$\frac{dk_r}{dt} = \frac{\partial D_o/\partial r}{\partial D_o/\partial \omega} \quad , \tag{35d}$$

$$\frac{dm}{dt} = \frac{\partial D_o/\partial \theta}{\partial D_o/\partial \omega} \quad , \tag{35e}$$

$$\frac{dn}{dt} = \frac{\partial D_o/\partial \phi}{\partial D_o/\partial \omega} = 0 \quad . \tag{35f}$$

Equations 35(a) - 35(c) comprise the group velocity equation and Eqs. (35d) -(35f) are equivalent to a Snell's Law. Notice that the nonconstancy of m due to the lack of θ symmetry is reflected in Eq. (35e) and the constancy of n due to toroidal symmetry is reflected in Eq. (35f). Equations (35) can then be integrated numerically to obtain the ray trajectory in $(\underline{x},\underline{k})$ space which satisfies the local dispersion relation $D_o = 0$. Here the form $D_o = D_R(\underline{x},\underline{k},\omega) = 0$ given by Eq. (17) is used.

The wave absorption can be calculated by integrating rate equations for the power deposition simultaneously with the ray equations,

$$\frac{dP}{dt} = -2\gamma P \quad , \quad \gamma = \sum_p \gamma^{(p)} \quad . \tag{36}$$

Here P is the power in the heating wave and γ is the damping decrement of the wave $\gamma << \omega$. The subscript p denotes the various damping mechanisms included in γ with $p = e,i,\ell$ for electron Landau damping, ion Landau damping, and collisional damping respectively. γ is calculated in a manner similar to that used for the spatial damping in Sec. IID by writing $D(\underline{x},\underline{k},\omega-i\gamma)$ $= D_o(\underline{x},\underline{k},\omega - i\gamma) + i \sum_p D_I^{(p)}(\underline{x},\underline{k},\omega - i\gamma)$, where D_o and $D_I^{(p)}$ are real for $\gamma = 0$. Expanding D for small γ and $D_I^{(p)}$ and assuming $D_o(\underline{x},\underline{k},\omega) = 0$ yields,

$$\gamma^{(p)} = \frac{D_I^{(p)}(\underline{x},\underline{k},\omega)}{(\partial D_o/\partial\omega)_\omega} \quad . \tag{37}$$

The forms for $D_I^{(p)}$ used in Eq. (37) are given by Eqs. (21a), (22), and (26).

IV. Numerical Results For Toroidal Ray Tracing

The ray equations and deposition equations can be integrated numerically [16,35-42], using an equilibrium constructed from Shafranov's aspect ratio expansion [32] with a lowest order cylindrical equilibrium of the form,

(i) Valid for $0 \leq r \leq a$,

$$N(r) = (N_o - N_a) \frac{e^{\xi_n} - e^{\xi_n (r/a)^2}}{e^{\xi_n} - 1} + N_a \quad , \tag{38a}$$

$$T_e(r) = (T_{eo} - T_{ea}) \frac{e^{-\xi_e (r/a)^2} - e^{-\xi_e}}{1 - e^{-\xi_e}} + T_{ea} \quad , \tag{38b}$$

$$T_i(r) = (T_{io} - T_{ia}) \frac{e^{-\xi_i (r/a)^2} - e^{-\xi_i}}{1 - e^{-\xi_i}} + T_{ia} \quad , \tag{38c}$$

$$B_\theta(r) = q_o^{-1} (r/R_o) B_o [1 + \xi_B (r/a)^2]^{-1} \quad , \tag{38d}$$

(ii) Valid for $a \leq r \leq a_w$,

$$N(r) = N_a \frac{a_w - r}{a_w - a} \quad , \tag{39a}$$

$$T_e(r) = (T_{ea} - T_{ew}) \frac{a_w - r}{a_w - a} + T_{ew} \quad , \tag{39b}$$

$$T_i(r) = (T_{ia} - T_{iw}) \frac{a_w - r}{a_w - a} + T_{iw} \quad , \tag{39c}$$

$$B_\theta(r) = B_\theta(r=a)(a/r) \quad . \tag{39d}$$

Here ξ_n, ξ_e, ξ_i, and ξ_B are all specified profile constants, q_o is the value of the safety factor at r=0; N_o, T_{eo}, T_{io} are respectively the central electron density, electron temperature, and ion temperature; N_a, T_{ea}, T_{ia} are respectively the electron density, electron temperature, and ion temperature at the limiter radius r=a; and T_{ew}, T_{iw} are respectively the electron and ion temperatures at the virtual limiter (or plasma wall radius, $r=a_w$).

Case A: The first case studied is for parameters typical of the Versator II lower hybrid heating experiment with a = 13 cm, a_w = 15.5 cm, R_o = 40 cm, $\omega/2\pi$ = 0.8 GHz, B_o = 14 KG, I_ϕ = 50 kA, T_{eo} = 400 eV, T_{io} = 150 eV, $T_{ea} = T_{ia}$ = 20 eV, $T_{ew} = T_{iw}$ = 10 eV, $N_o = 2\times10^{13}$ cm^{-3}, $N_a = 2\times10^{12}$ cm^{-3}, q_o = 1.0, ξ_e = 3.94, ξ_i = 3.94, ξ_n = 0.1, Z_e = 2.0, and hydrogen ions. A toroidal mode number n = 44.6 was chosen which corresponds to an initial value of $n_\parallel^{(o)}$=5.0 . For these parameters the slab theory of Sec. II predicts that $n_a \simeq 1.85$ for accessibility so that initially $n_\parallel^{(o)} > n_a$. The linear limit $[x_{oe}^{(c)} \lesssim 2.8]$ and quasilinear limit $[x_{oe}^{(c)} \lesssim 2.3]$ for electron Landau damping that were derived in Sec. II imply critical values of $n_\parallel \equiv n_\parallel^{(c)}$ for Landau damping at a given temperature of the form,

$$n_\parallel^{(c)}{}_L \gtrsim \frac{5.7}{[T_e(\text{keV})]^{1/2}} \quad , \tag{40a}$$

$$n_\parallel^{(c)}{}_{QL} \gtrsim \frac{7.0}{[T_e(\text{keV})]^{1/2}} \quad . \tag{40b}$$

For the chosen parameters, Eqs. (40) give $n_\parallel^{(c)}{}_L \gtrsim 9.0$ and $n_\parallel^{(c)}{}_{QL} \gtrsim 11.1$ for electron damping at r=0. Equation (19) can be inverted to give a critical

value of $n_{\parallel} \equiv n_{\parallel}^{(c)}|_{MC}$ at which ion mode conversion and Landau damping should occur,

$$n_{\parallel}^{(c)}|_{MC} = \frac{6.5}{T_i^{1/2}(keV)} \left[1 + \frac{1}{4}\frac{T_e}{T_i}\Omega^4\right]^{-1/2} \left[\frac{\omega^2}{\omega_{LH}^2(r_{MC})} - 1\right] \quad . \qquad (41)$$

For the chosen parameters, (41) predicts $n_{\parallel}^{(c)}|_{MC} = 7.50$ at the plasma center ($r_{MC} = 0$). Since $n_{\parallel}^{(o)} = 5.0$, the results of Sec. II would predict no electron or ion Landau damping of the incident lower hybrid wave.

In Figs. 3(a) - 3(e) the results are shown for a ray trajectory which is started at the plasma edge on the low magnetic field side of the tokamak with $r \simeq 1.15a$, $\theta = 0$, $m = 0$, $\phi = 0$, and k_r calculated to satisfy $D_R(r,\theta\ ;\ k_r, m,n,\omega) = 0$. Picking the initial condition $m = 0$ implies a poloidally symmetric antenna where the incident waveform is not dependent on θ (or alternately where the vertical dimension of the waveguide is greater than the plasma minor radius). However these conditions are not always satisfied, in which case one might use cone theory [9,10] (as mentioned in Sec. II) to accurately reconstruct the electric field in the plasma due to a particular antenna structure. From Figs. 3(b) and 3(c) it can be seen that as the ray propagates from $\theta = 0$ to $\theta = \pi$, m decreases from $m = 0$ to $m = -85$ and $n_{\parallel}$ likewise decreases from $n_{\parallel} = 5.0$ to $n_{\parallel} = 2.0$. The ray then undergoes a radial reflection ($k_r \to 0$) in the plasma interior and propagates out to the plasma edge, unable to satisfy any of the local conditions for wave absorption [Eqs. (40) - (41)]. The ray finally undergoes a radial reflection at the plasma edge near $\theta \simeq -\pi/2$ and m increases rapidly from $m = -120$ to $m = 100$ as the ray propagates inward. Correspondingly, $n_{\parallel}$ increases from $n_{\parallel} = 2$ to $n_{\parallel} \simeq 13$. From Figs. 3(d) - 3(e) it can be seen that at the point of absorption $x_{oe} \tilde{\simeq} 2.8$ and $x_{oi} \simeq 3.4$. During this final pass into the plasma

interior the wave damps 70% of its power to plasma electrons at a radial location $0.35 \lesssim r/a \lesssim 0.6$, and none of the wave power is absorbed on plasma ions. As the wave propagates along its entire trajectory, 29% of its power was damped nonresonantly due to collisions at a radial location $0.4 \lesssim r/a \lesssim 1.1$.

Case B: A sharp contrast to Case A is shown in Figs. 4(a) - 4(e). Case B is identical to Case A except that the ray is launched from a position in the poloidal plane defined by $\theta = 3\pi/2$. -see Fig. 4(a). Clearly the ray damps on its first pass to the plasma center, with m increasing from m = 0 to m = 60 [Fig. 4(b)] and $n_{||}$ increasing from $n_{||} = 5.0$ to $n_{||} = 9.0$ [Fig. 4(c)]. The corresponding values of $x_{oe} \simeq 2.7$ and $x_{oi} \simeq 2.9$ at the end of the ray can be seen in Figs. 4(d) - 4(e). Here 67% of the wave power is damped due to electron Landau damping in a radial location $0.05 \lesssim r/a \lesssim 0.25$, 21% of the wave power is damped due to ion Landau damping in a radial location $0.05 \lesssim r/a \lesssim 0.25$, and 11% of the wave power is damped collisionally.

The behavior observed in Cases A and B can be understood in the following way [16,37,40,43]. Consider a simplified model using the cold plasma, electrostatic dispersion relation Eq. (12), $\underline{B} = \underline{e}_z B_o + \underline{e}_\theta B_\theta(r)$, $B_\phi \simeq B_o/[1 + (r/R_o)\cos\theta]$, and $N = N(r)$. Then $k_\perp^2$ and $k_{||}^2$ are given by $k_\perp^2 \simeq k_r^2 + [(m/r) - (n/R)B_\theta/B_\phi]^2$ and $k_{||} \simeq [(m/r)B_\theta/B_\phi + (n/R)]$. The ray equations can then be used to calculate the instantaneous value of $dm/d\theta$,

$$\frac{dm}{d\theta} = -\frac{\partial D_o/\partial\theta}{\partial D_o/\partial m} \simeq -k_{||} R_o q(r) \left[1 + \frac{\omega_{pe}^2/\Omega_{ce}^2}{\varepsilon_\perp}\right] \frac{r}{R} \sin\theta \quad , \tag{42}$$

where $q(r)$ is the local safety factor, $q(r) = rB_o/(R_o B_\theta)$. Clearly for $k_{||} > 0$ and $q(r) > 0$, the value of $dm/d\theta$ is positive and maximum near $\theta = 3\pi/2$ whereas for $0 \lesssim \theta \lesssim \pi/2$ the value of $dm/d\theta$ is negative. This would explain why rays launched near $\theta = 0$ have their m numbers and values of $n_{||}$ downshifted

initially, whereas rays launched near $\theta = 3\pi/2$ undergo immediate upshifts in m and $n_{||}$. In fact the ray launched in Case A exhibits the same behavior along the final part of its trajectory (final edge reflection near $\theta = 3\pi/2$) that the ray in Case B showed initially. Note that if the sign of the toroidal mode number ($k_{||}$) were reversed or the sign of the toroidal current (B_θ) were reversed, then the point corresponding to a maximum positive value of $dm/d\theta$ would be $\theta = \pi/2$ [see Eq. (42)]. This purely toroidal effect is the basis of a top launching waveguide structure being tested on the Versator II lower hybrid heating experiment at MIT [44].

V. Simulation Model for Lower Hybrid Heating

A detailed simulation model has been developed [45] to study lower hybrid heating, incorporating the various theories of wave propagation and wave absorption discussed in Secs. II - IV into a transport code [46]. Here a brief description of this simulation model is given along with a numerical example relevant to the Alcator C lower hybrid heating experiment.

A. Transport Code

The radial transport code [46] consists of a set of mass and energy conservation equations for ions and electrons. For simplicity, the density profile is taken to be constant in time (no density transport). The electron and ion energy conservation equations include source terms due to the electron and ion Landau damping and collisional damping of a longitudonal ($k_{\parallel}$) spectrum of lower hybrid waves launched at the plasma edge. Also included is a source due to electron-ion collisional equilibration [47] and a source due to ohmic heating. The ion thermal conductivity is of the form $\chi_i = (3\text{-}5)\chi_i^{(NEO)}$, where $\chi_i^{(NEO)}$ is the neoclassical ion conductivity of Hinton and Hazeltine [48]. The electron thermal conductivity is taken to be of the form [49] $\chi_e \alpha B_\theta(r)(a/r)/(N^{4/5}T_e)$ for the ohmically heated plasma. When the RF is turned on, χ_e is taken to be of the same form as above, except that it is evaluated using the value of ohmic temperature $T_e^{(OH)}(r)$ before the RF was turned on.

B. Poloidal Field Evolution

The evolution of the poloidal field is determined from Maxwell's Equations and Ohm's Law. A Spitzer resistivity is assumed [50].

C. Quasilinear Calculation

The one dimensional (parallel velocity) Fokker Planck equation given in Sec. IIF [Eq. (27)] is solved assuming steady state ($\partial F/\partial t = 0$), at each radial location of the plasma. The resulting electron distribution function $F(r,v_{||})$ is used in the toroidal ray tracing to evaluate the electron Landau damping. The quasilinear diffusion coefficient $D_{q\ell} \alpha P(n_{||})$ is evaluated using the toroidal ray tracing.

D. Toroidal Ray Tracing

The ray equations and rate deposition equations (35) - (37) are solved using the thermal, electromagnetic dispersion relation (17). A Shafranov equilibrium is calculated based on the zeroth order cylindrical equilibrium of the transport code [actually the transport code quantities $N(r)$, $T_e(r)$, $T_i(r)$ and $B_\theta(r)$ are fitted first to Eqs. (38) - (39)]. The resonant and nonresonant wave absorption is evaluated using the results of Sec. II, Eqs. (21a), (22), and (26). The electron Landau damping contribution (21a) is evaluated using the resulting quasilinear F rather than a Maxwellian,

$$D_I^{(e)} = -\pi c^2 \frac{\omega_{pe}^2}{\omega^2} n_\perp^2 \frac{\partial F}{\partial v_{||}} \quad , \tag{43}$$

where F has been normalized so that $F(v_{||} = 0) = (2\pi)^{-1/2} v_e^{-1}$. A Maxwellian distribution function is assumed for the ions (for all time) so that the form given for $D_I^{(i)}$ in Eq. (22) is appropriate. The interaction of the three units of the simulation model can be summarized as follows. The transport code first advances the quantities N, T_e, T_i, and B_θ. The toroidal ray tracing calculates source terms and a $D_{q\ell}(v_{||})$ based on these transport quantities assuming initial Maxwellian distribution functions for

both ions and electrons. The Fokker Planck code then calculates a quasilinear distribution F for the electrons based on the initial $D_{q\ell}(v_{\|})$. The transport quantities are then advanced in time and the toroidal ray tracing is repeated using the new quasilinear F to calculate the sources and a new $D_{q\ell}(v_{\|})$.

D. Numerical Results

Here numerical results are presented for parameters relevant to the Alcator C lower hybrid heating experiment operating in the electron heating mode. A spectrum of lower hybrid waves calculated using a Brambilla code [1] is launched at the plasma edge. The spectrum is characterized by the longitudinal wavenumber or index of refraction $n_{\|}$ and is given by

$$P(n_{\|}) = P_o \exp\left[-\alpha_p(|n_{\|}|-n_o)^2\right] \quad , \tag{44}$$

where $\alpha_p \simeq 4.0$, $n_o = 3.0$, and P_o is chosen so that

$$\int_{-\infty}^{\infty} P(n_{\|})dn_{\|} = P_{IN} \quad ,$$

where P_{IN} is the total input power. For the example given, $P_{IN} = 0.5$ MW and Eq. (44) corresponds approximately to the power spectrum launched by the Alcator C four waveguide grill phased $0\text{-}\pi\text{-}0\text{-}\pi$. Other parameters are $a = 16.5$ cm, $R_o = 64$ cm, $\omega/2\pi = 4.6$ GHz, $B_o = 90$ kG, $I_\phi = 410$ kA, $T_{eo}^{(OH)} \simeq 2000$ eV, $T_{io}^{(OH)} \simeq 1000$ eV, $T_{ea} = T_{ia} = 30$ eV, $a_w = 17.8$ cm, $T_{ew} = T_{iw} = 5$ eV, $N_o = 1.91\times10^{14}$ cm^{-3}, $N_a = 5.73\times10^{13}$ cm^{-3}, $q_o \simeq 1.0$, $\xi_n \simeq 0.44$ (corresponding to a circular density profile), $Z_e = 1.5$, and deuterium ions. The input Brambilla power spectrum is divided into 32 components in the ranges $-4.63 \leq n_{\|} \leq -1.33$ and $1.33 \leq n_{\|} \leq 4.63$, with spacing $\Delta n_{\|} = 0.22$. For the chosen parameters,

Eqs. (11) predict an accessible $n_{\parallel} \equiv n_a = 1.53$, so that most of the launched power should be accessible to the plasma interior. During the simulation, the RF was turned on for a pulse length $\Delta T_{RF} = 70$ msec.

Before proceeding to discuss the simulation results, a typical ray trajectory has been shown for these Alcator C parameters in Figs. 5(a) - 5(b). The damping for this ray is based on a Maxwellian distribution for both electrons and ions and $\xi_e = \xi_i = 3.11$ has been assumed for the electron and ion temperature profiles. A toroidal mode number $n = 23.2$ has been chosen corresponding to an initial $n_{\parallel}^{(o)} = 3.0$ (maximum of power spectrum). The ray trajectory and $n_{\parallel}$ behavior are similar to that found in Sec. IV. The ray damped 68% of its power resonantly on electrons in a radial location $0.1 \lesssim r/a \lesssim 0.4$ and the remaining 31% of its power nonresonantly due to collisions in a radial location $0.6 \lesssim r/a \lesssim 1.05$. The highest value of $n_{\parallel} = 5.0$ represents a considerable upshift from the initial value of $n_{\parallel}^{(o)} = 3.0$ and the final value of $x_{oe} \gtrsim 3.0$ is consistent with the linear Landau damping theory.

The results of the numerical simulation model are shown in Figs. 6(a) -6(c). Figure 6(a) is the central electron and ion temperatures versus time. The RF is turned on at $T \equiv T_{RF} = 100$ msec where $T_{eo}^{(OH)} \simeq 2080$ eV and $T_{io}^{(OH)} \simeq 1180$ eV. The increase in central electron temperature is $\Delta T_{eo} \simeq 276$ eV and the increase in central ion temperature is $\Delta T_{io} \simeq 83$ eV [Fig. 6(a)]. These temperature increases are consistent with those reported experimentally [51] at the $P_{RF} = 500$ KW level in Alcator C using graphite limiters. The rise in electron temperature is mostly due to resonant electron Landau damping and the ion temperature increase is due to collisional equilibration with the electrons. Figure 6(b) is a plot of the integrated RF power as a function of radius and corresponds to a time 5 msec after the RF

is turned on. The interesting aspect of this figure is that only 200 KW out of the initial 500 KW of RF power is damped resonantly due to electron Landau resonance in the inner half of the plasma ($r \lesssim 8$ cm). The remaining 300 KW is damped nonresonantly due to collisions in the outer half of the plasma. This effect is a result of the high edge density ($N_a = 0.3\ N_o$). Figure 6(c) is a plot of the quasilinear electron distribution function F showing in detail the region where the plateau has formed (region of power). F has been conveniently plotted as a function of the kinetic energy E where

$$E = m_e c^2\ [\gamma - 1] \quad , \quad \gamma = [1 - n_{\parallel}^{-2}]^{-1/2} \quad . \tag{47}$$

The plot is at a radius $r = 1.03$ cm and corresponds to a time 1 msec after the RF is turned on (T_{RF}). The endpoints of the plateau are worth examining. The low phase velocity endpoint is given by $E \simeq 12$ keV which corresponds to $n_{\parallel} \simeq 4.62$. The electron temperature at this radius is $T_e \simeq 2098$ eV which gives a value of $x_{oe} = \omega/(\sqrt{2} k_{\parallel} v_e) \simeq 2.37$. Thus the lower hybrid wave spectrum does indeed penetrate to a lower parallel phase velocity (or higher temperature) before being absorbed via electron Landau damping - just as predicted by the quasilinear theory of Sec. II. The high phase velocity endpoint is given by an energy $E \simeq 158$ keV which corresponds to $n_{\parallel} \simeq 1.55$. The critical value of $n_{\parallel}$ for accessibility at this density and magnetic field is $n_a \simeq 1.5$. This agrees with the endpoint value of $n_{\parallel} = 1.55$ to within the accuracy of the grid in $n_{\parallel}$ space on which the quasilinear calculation was done ($\Delta n_{\parallel} = 0.22$).

VI. Summary

A review of the slab model of wave propagation was given, including the topics of accessibility and linear ion mode conversion. The linear theories of ion and electron Landau damping and quasilinear theory of electron Landau damping for the lower hybrid wave were also reviewed. The extension of the wave propagation theory to toroidal geometry was then presented. It was found that global predictions of wave accessibility and wave absorption were no longer possible because of variations in $k_{\parallel}$ due to the two dimensional (r,θ) inhomogeneity present in realistic tokamak equilibria. Finally a simulation model was described which combines a radial transport code with a toroidal ray tracing code and Fokker Planck calculation. As already mentioned in the Introduction, nonlinear effects and the effect of density fluctuations were not discussed. It is worth pointing out however, that density fluctuations have been verified experimentally in PLT [52] and in Alcator A and Alcator C [53,54]. Extensive theoretical work [55,56,57] has been done which indicates that scattering of the lower hybrid wave from density fluctuations can result in significant rotation of the incident wave $\underline{k}_{\perp}$ vector. This effect combined with magnetic shear and toroidal m variations can significantly alter the accessibility and absorption of the lower hybrid wave.

VII. Acknowledgements

I would like to acknowledge very useful and informative discussions with Professor Miklos Porkolab, Dr. Ronald Englade, Dr. Steven Knowlton, Dr. Geoffrey Crew, Dr. Linda Sugiyama, and Professor Bruno Coppi.

REFERENCES

[1] R.R. Parker, Massachusetts Institute of Technology, Research Laboratory of Electronics, Report QPR 102, 97 (1971); W. Hooke, International School of Plasma Physics, Varenna 1971, (EUR-5064, p. 310 Luxembourg 1974); A. Bers, Proceedings of the Third Topical Conference on Radio Frequency Plasma Heating (Pasadena, California, 1978) Paper A-1.

[2] T.H. Stix, The Theory of Plasma Waves (McGraw-Hill, Inc., New York, 1962).

[3] F. Troyon and F.W. Perkins, Proceedings of the Second Topical Conference on Radio Frequency Plasma Heating (Texas Tech University, Lubbock, Texas, 1974) Paper B4.

[4] M. Brambilla, Nuclear Fusion 14, 327 (1974).

[5] M. Porkolab, Fusion, edited by Edward Teller (Academic Press, New York, 1981) Chapter 13.

[6] V.E. Golant, Zh. Tekh. Fiz. 41, 2492 (1971) [Sov. Phys. Tech. Phys. 16, 1980 (1972)].

[7] H.H. Kuehl, Physics of Fluids 5, 1095 (1962).

[8] P.M. Bellan, and M. Porkolab, Physics of Fluids 19, 995 (1976).

[9] P.L. Colestock, Nuclear Fusion 18, 740 (1978).

[10] P.M. Bellan, Physics of Fluids 16, 741 (1983).

[11] R.K. Fisher, and R.W. Gould, Physical Review Letters 22, 1093 (1969).

[12] R.J. Briggs, and R.R. Parker, Physical Review Letters 29, 852 (1972).

[13] N.A. Krall, and A.W. Trivelpiece, Principles of Plasma Physics (McGraw-Hill, Inc., New York, 1973), Chapter 8.

[14] T.H. Stix, Physical Review Letters 15, 878 (1965).

[15] M. Brambilla, Plasma Physics 18, 669 (1976).

[16] D.W. Ignat, Physics of Fluids 24, 1110 (1981).

[17] J.P.M. Schmitt, J. Plasma Physics 12, 51 (1974).

[18] V.M. Glagolev, Plasma Physics 14, 301 (1972).

[19] K. Ko, A. Bers, and V. Fuchs, Proceedings of the Fourth Topical Conference on Radio Frequency Plasma Heating (University of Texas, Austin, TX, 1981) Paper C-17.

[20] A.H. Glasser, Bulletin of the American Physical Society 25, 1001 (1980).

[21] M.D. Simonutti, Physics of Fluids 18, 1524 (1975).

[22] D.E. Baldwin and G. Rowlands, Physics of Fluids 9, 2444 (1966).

[23] C.F.F. Karney, Physics of Fluids 21, 1584 (1978).

[24] C.F.F. Karney and A. Bers, Physical Review Letters 39, 550 (1977).

[25] C.F.F. Karney, Physics of Fluids 22, 2188 (1979).

[26] M. Brambilla, Proceedings of the Physics of Plasmas Close to Thermonuclear Conditions, Varenna, Italy, 1979 (C.E.C., Brussels, 1980), Vol. I 291.

[27] A. Bers, F.W. Chambers, and N.J. Fisch, M.I.T. Plasma Research Report PRR-76/23 (1976).

[28] C.F.F. Karney and N.J. Fisch, Physics of Fluids 22, 1817 (1979).

[29] M. Brambilla, Nuclear Fusion 16, 47 (1976); V. Krapchev and A. Bers, Nuclear Fusion 18, 519 (1978); M. Brambilla, Nuclear Fusion 19, 1343 (1979); A. Bers and K. Theilhaber, Nuclear Fusion 23, 41 (1983).

[30] R.C. Davidson, Methods in Nonlinear Plasma Theory (Academic Press, New York, 1972) pp. 159-161.

[31] N.J. Fisch, Physical Review Letters 41, 873 (1978).

[32] V.D. Shafranov, Reviews of Plasma Physics, edited by M.A. Leontovich (Consultants Bureau, New York, 1966) Vol. 2.

[33] L.D. Landau and E.M. Lifshitz, The Classical Theory of Fields (Pergamon Press, Oxford, 1979) Chapter 7.

[34] S. Weinberg, Physical Review 126, 1899 (1962).

[35] J.M. Wersinger, E. Ott, and J.M. Finn, Physics of Fluids 21, 2263 (1978).

[36] Yu. F. Baranov and V.I. Fedorov, Pis'ma Zh. Tekh. Fiz. 4, 800 (1978) [Soviet Phys.-Tech. Phys. Lett. 4, 322 (1978)].

[37] Yu. F. Baranov and V.I. Fedorov, Nuclear Fusion 20, 1111 (1980).

[38] J.L. Kulp, Bulletin of the American Physical Society 23, 789 (1978); J.L. Kulp, Ph.D. dissertation, Massachusetts Institute of Technology (1978).

[39] E. Ott, J.M. Wersinger, and P.T. Bonoli, Physics of Fluids 22, 192 (1979).

[40] P.T. Bonoli and E. Ott, Physics of Fluids 25, 359 (1982).

[41] T. Maekawa, Y. Terumichi, and S. Tanaka, IEEE Trans. Plasma Science PS-8, 2 (1980).

[42] S. Ejima, V.S. Chan, R. La Haye, C. Moeller, P.I. Petersen, and J.C. Wesley, Bulletin of the American Physical Society 22, 1170 (1977).

[43] P.L. Colestock, and J.L. Kulp, IEEE Trans. Plasma Science PS-8, 71 (1980).

[44] S.F. Knowlton et al., Bulletin of the American Physical Society 28, 1236 (1983).

[45] R. Englade, P.T. Bonoli, and T.M. Antonsen, Proceedings of the Fourth Topical Conference on Radio Frequency Plasma Heating (University of Texas, Austin, Texas, 1981) Paper C-14.

[46] T. Antonsen, B. Coppi, and R. Englade, Nuclear Fusion 19, 641 (1979).

[47] S.I. Braginskii, Reviews of Plasma Physics, edited by M.A. Leontovich (Consultants Bureau, New York, 1965) Vol. 1.

[48] F.L. Hinton and R.D. Hazeltine, Reviews of Modern Physics 48, 239 (1976).

[49] B. Coppi and E. Mazzucato, Physics Letters 71A, 337 (1979).

[50] F.L. Hinton, J.C. Wiley, D.F. Düchs, H.P. Furth, and P.H. Rutherford, Physical Review Letters 29, 698 (1972).

[51] M. Porkolab et al., Proceedings of the Fifth Topical Conference on Radio Frequency Plasma Heating (University of Wisconsin, Madison, Wisconsin, 1983) p. 88.

[52] E. Mazzucato, Physical Review Letters 36, 792 (1976).

[53] R.E. Slusher, C.M. Surko, J.J. Schuss, R.R. Parker, I.M. Hutchinson, D. Overskei, and L.S. Scaturro, Physics of Fluids 3, 457 (1982).

[54] R.L. Watterson, C.M. Surko, and R.E. Slusher, Bulletin of the American Physical Society 27, 937 (1982).

[55] E. Ott, Physics of Fluids 22, 1732 (1979).

[56] P.T. Bonoli, and E. Ott, Physical Review Letters 46, 424 (1981).

[57] P.L. Andrews, and F.W. Perkins, Physics of Fluids 26, 2537 (1983).

FIGURE CAPTIONS

Figure 1: $n_\perp^2$ versus N for fixed $n_\parallel$ from Eq. (9). N_S and N_F denote densities corresponding to the slow and fast wave cutoffs. N_{T1} and N_{T2} denote densities corresponding to the confluence point for the slow and fast wave modes.

Figure 2: $n_\perp^2$ versus N for fixed $n_\parallel$ from Eq. (17). N_{MC} is the density corresponding to the ion mode conversion point defined by Eq. (19).

Figure 3: Ray Trajectory data for Versator II parameters with $n_\parallel = 5.0$ and $\theta = 0$ initially. (a) Ray trajectory in the $(r-\theta)$ plane, (b) Poloidal mode number m plotted versus θ, (c) Axial index of refraction $n_\parallel$ plotted versus θ, (d) $x_{oe} = \omega/(\sqrt{2}k_\parallel v_e)$ plotted versus θ, (e) $x_{oi} = \omega/(\sqrt{2}k_\perp v_i)$ plotted versus θ.

Figure 4: Ray trajectory data for Versator II parameters with $n_\parallel = 5.0$ and $\theta = 3\pi/2$ initially. (a) Ray trajectory in the $(r-\theta)$ plane, (b) Poloidal mode number m plotted versus θ, (c) Axial index of refraction $n_\parallel$ plotted versus θ, (d) $x_{oe} = \omega/(\sqrt{2}k_\parallel v_e)$ plotted versus θ, (e) $x_{oi} = \omega/(\sqrt{2}k_\perp v_i)$ plotted versus θ.

Figure 5: Ray trajectory data for Alcator C parameters with $n_\parallel = 3.0$ and $\theta = 0$ initially, (a) Ray trajectory in $(r-\theta)$ plane, (b) Axial index of refraction $n_\parallel$ plotted versus θ.

Figure 6: Lower hybrid heating simulation for Alcator C parameters. (a) Central electron temperature T_{eo} and central ion temperature T_{io} versus time T. The RF turn-on time is $T_{RF} = 100$ msec,

Fig. 6... (b) Integrated RF power versus radius r at a time T_{RF}+5 msec, (c) Electron distribution function F(E) versus kinetic energy E at a radius r=1.03 cm at a time T_{RF}+1 msec.

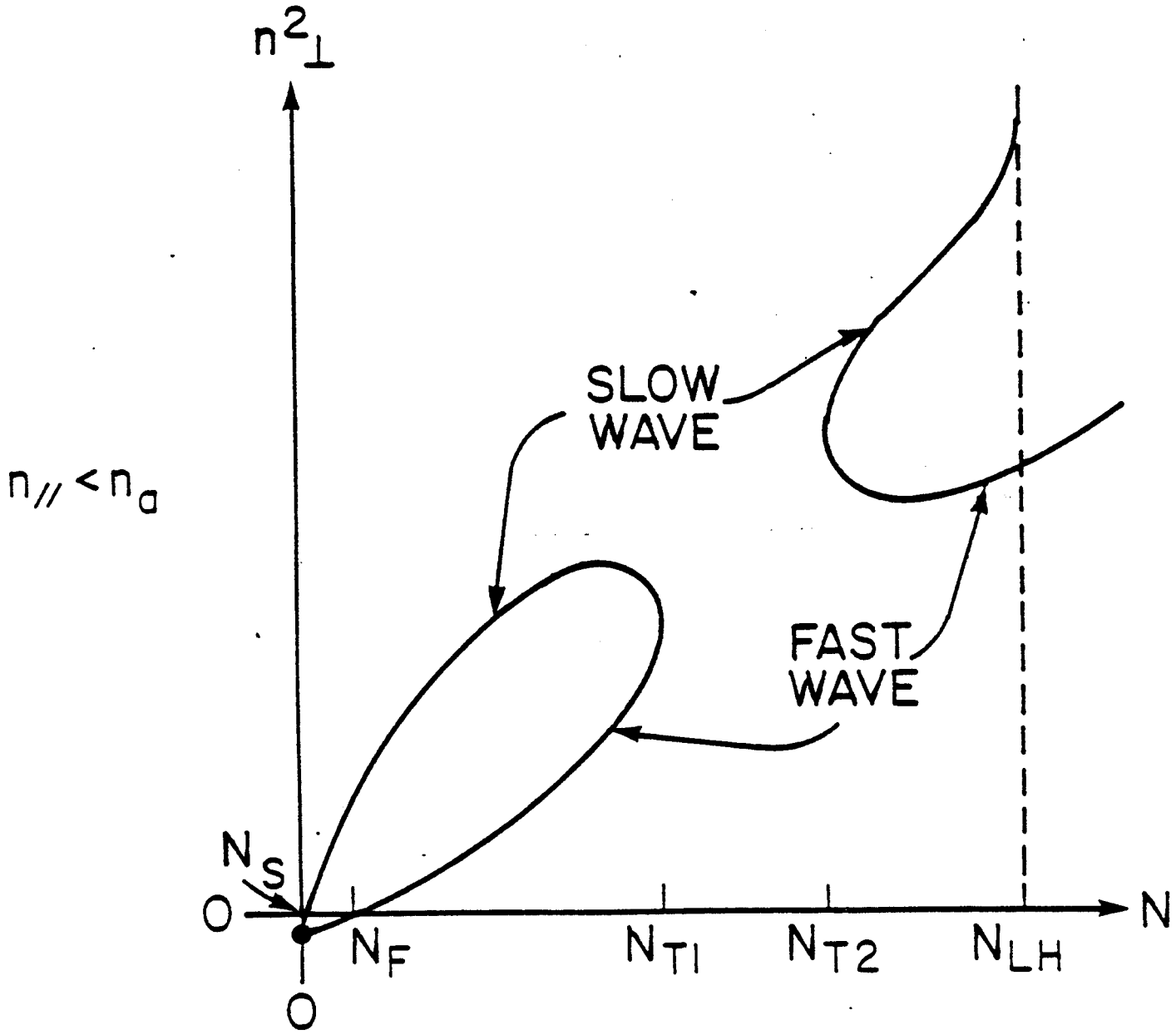

Figure 1(a).

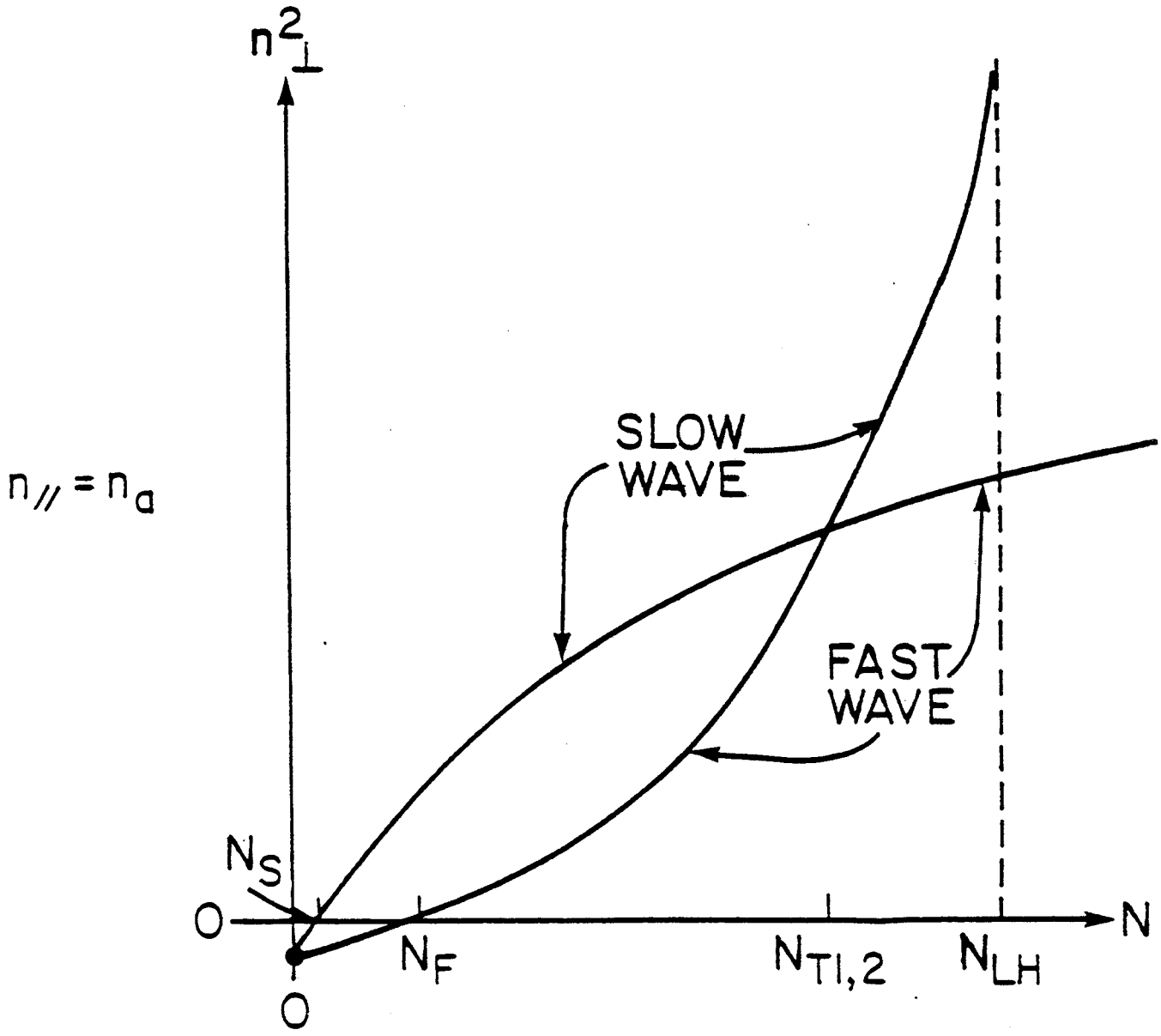

Figure 1(b).

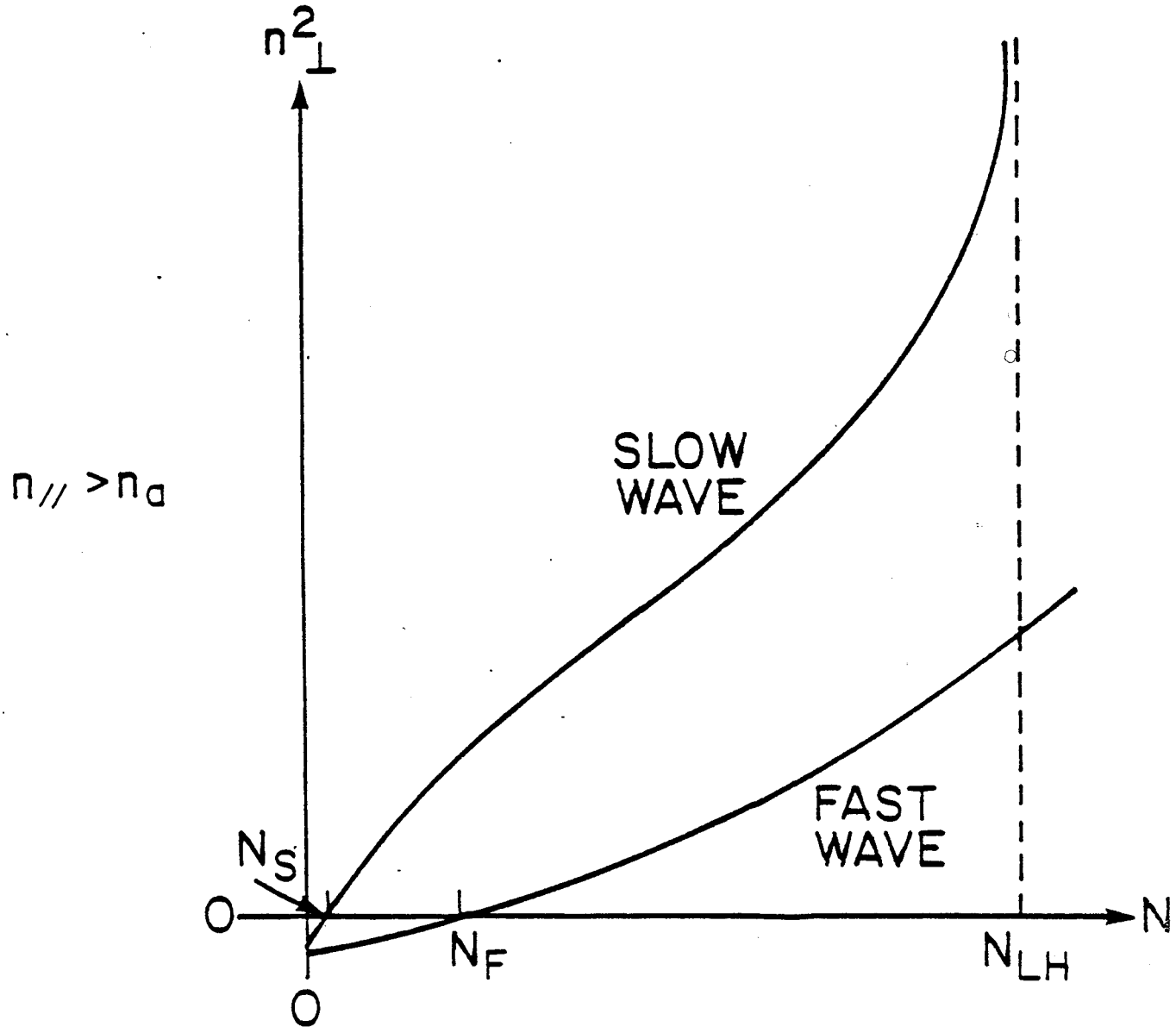

Figure 1(c).

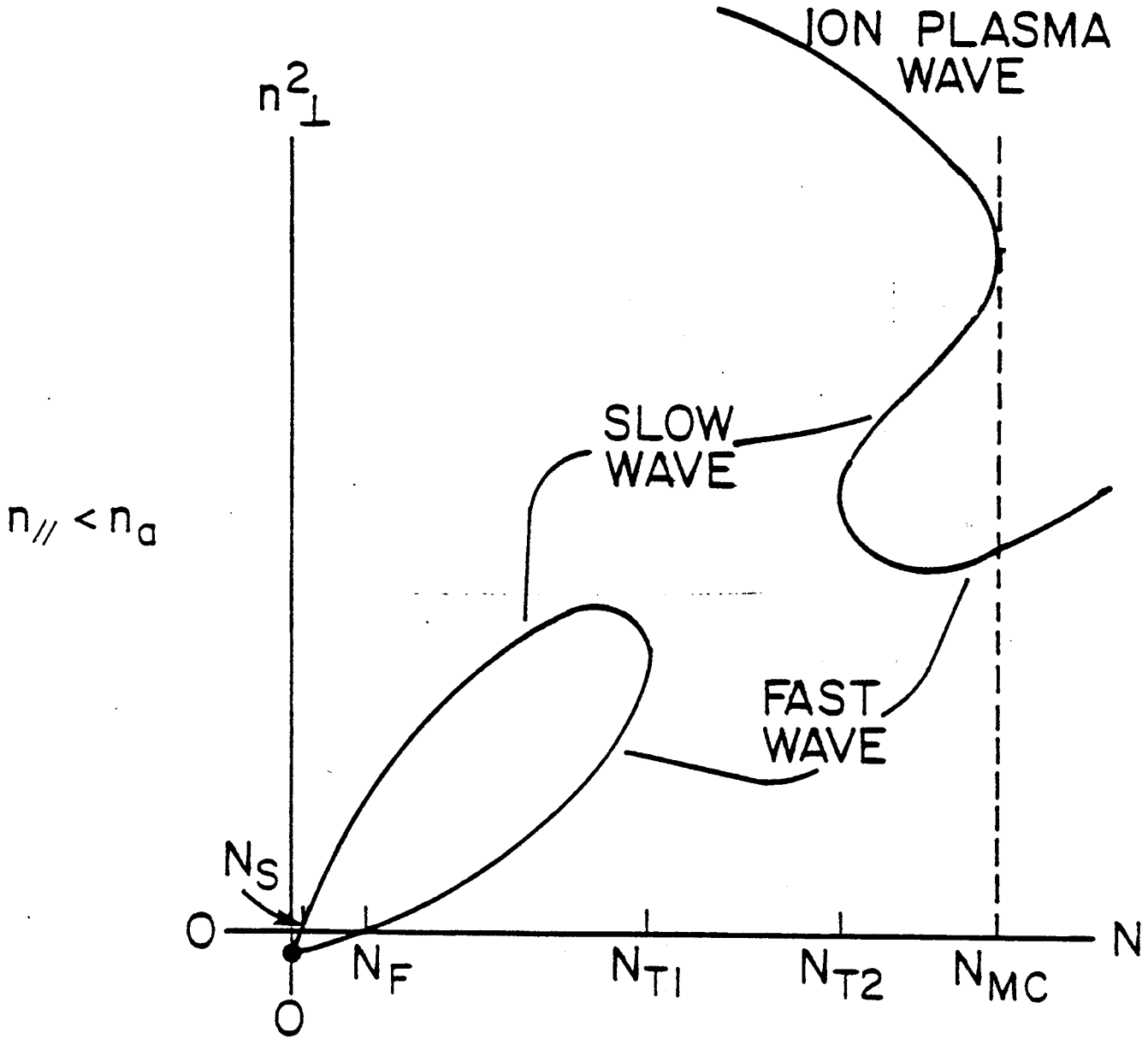
ION PLASMA
WAVE
$n^2_\perp$
SLOW
WAVE
$n_{//} < n_a$
FAST
WAVE
N_S
O
N_F
N_{T1}
N_{T2}
N_{MC}
N
O

Figure 2(a).

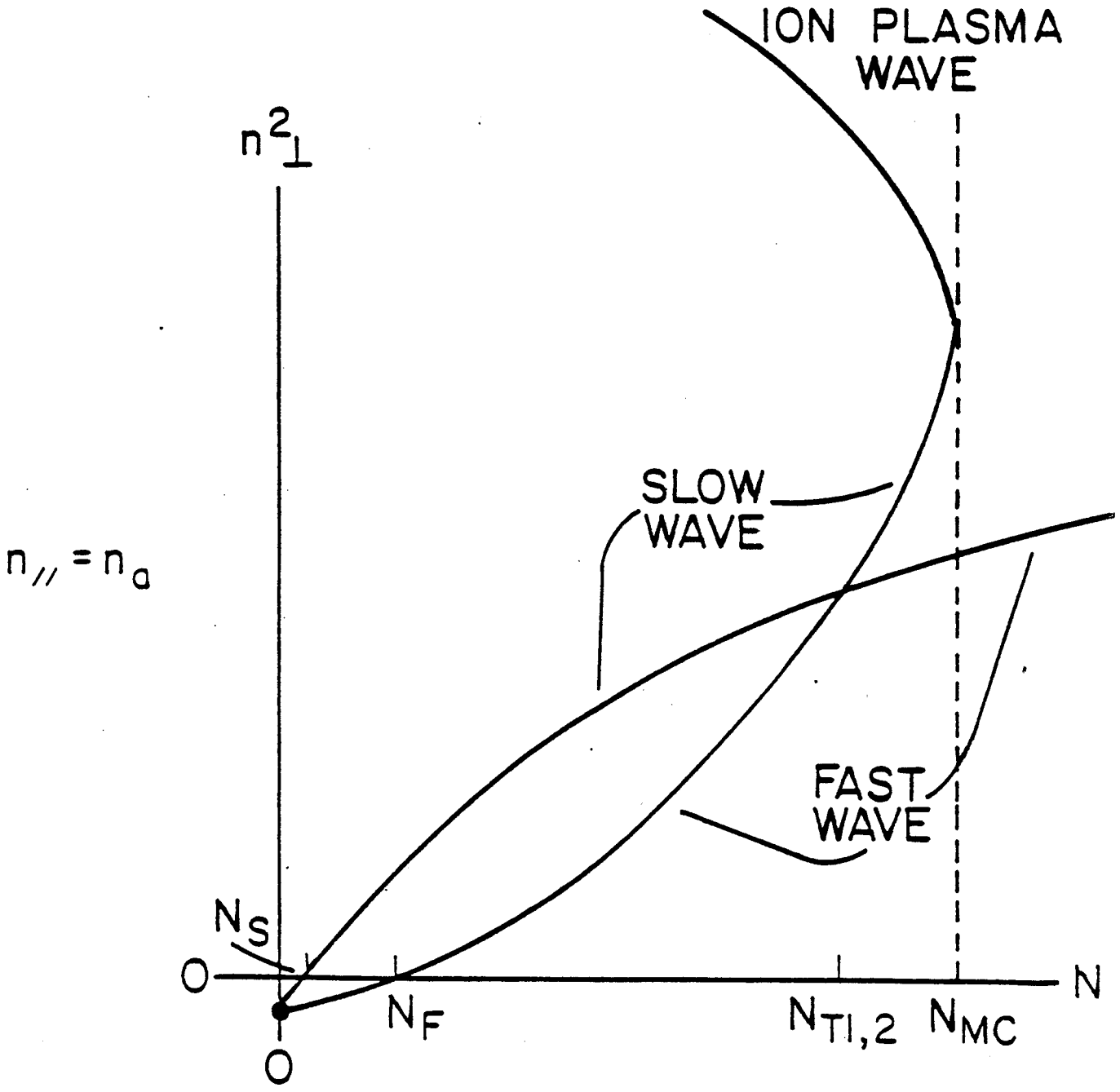
ION PLASMA
WAVE
$n^2_\perp$
SLOW
WAVE
$n_{//} = n_a$
FAST
WAVE
N_S
O
N_F
$N_{TI,2}$
N_{MC}
N
O

Figure 2(b).

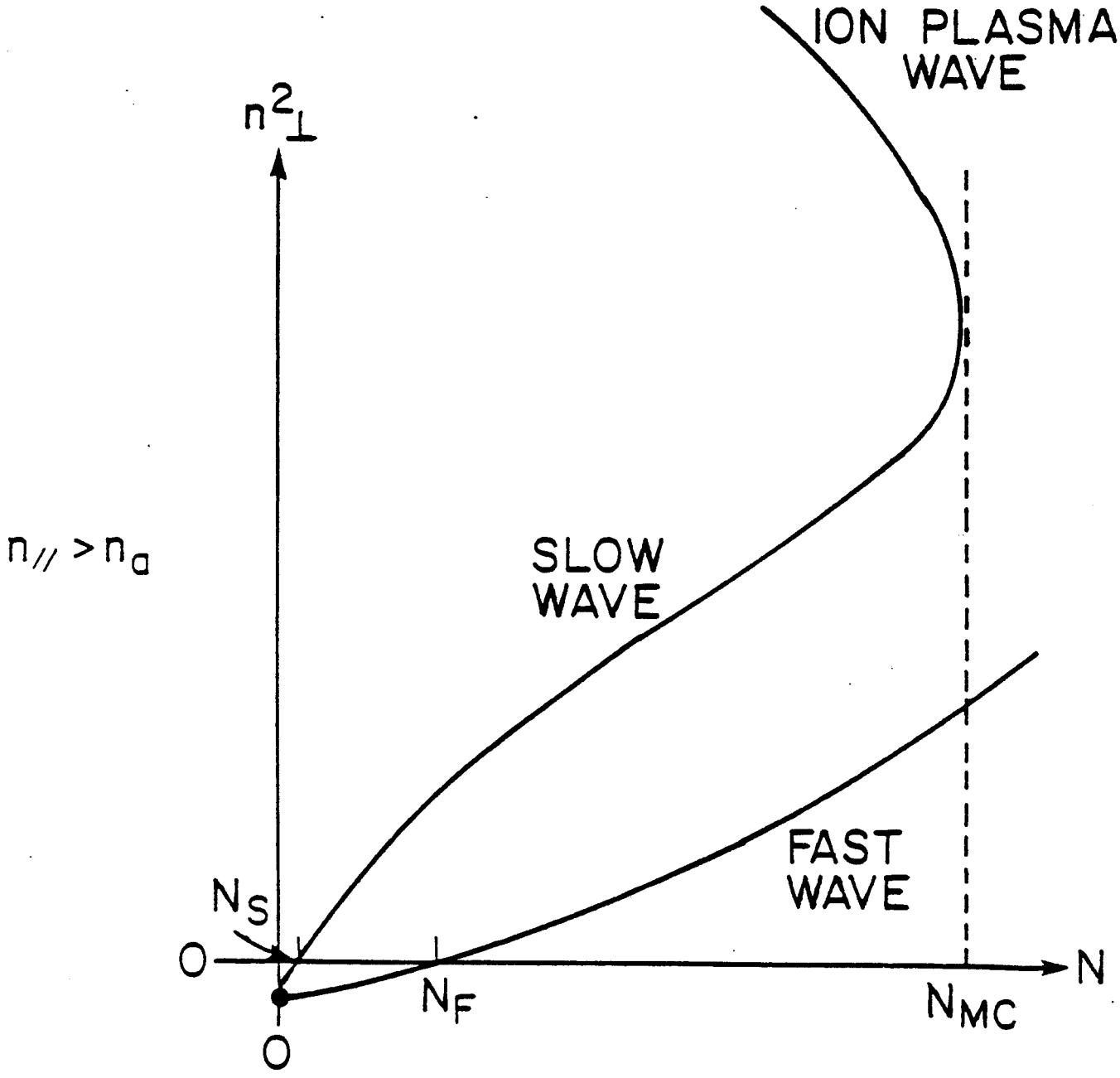

Figure 2(c).

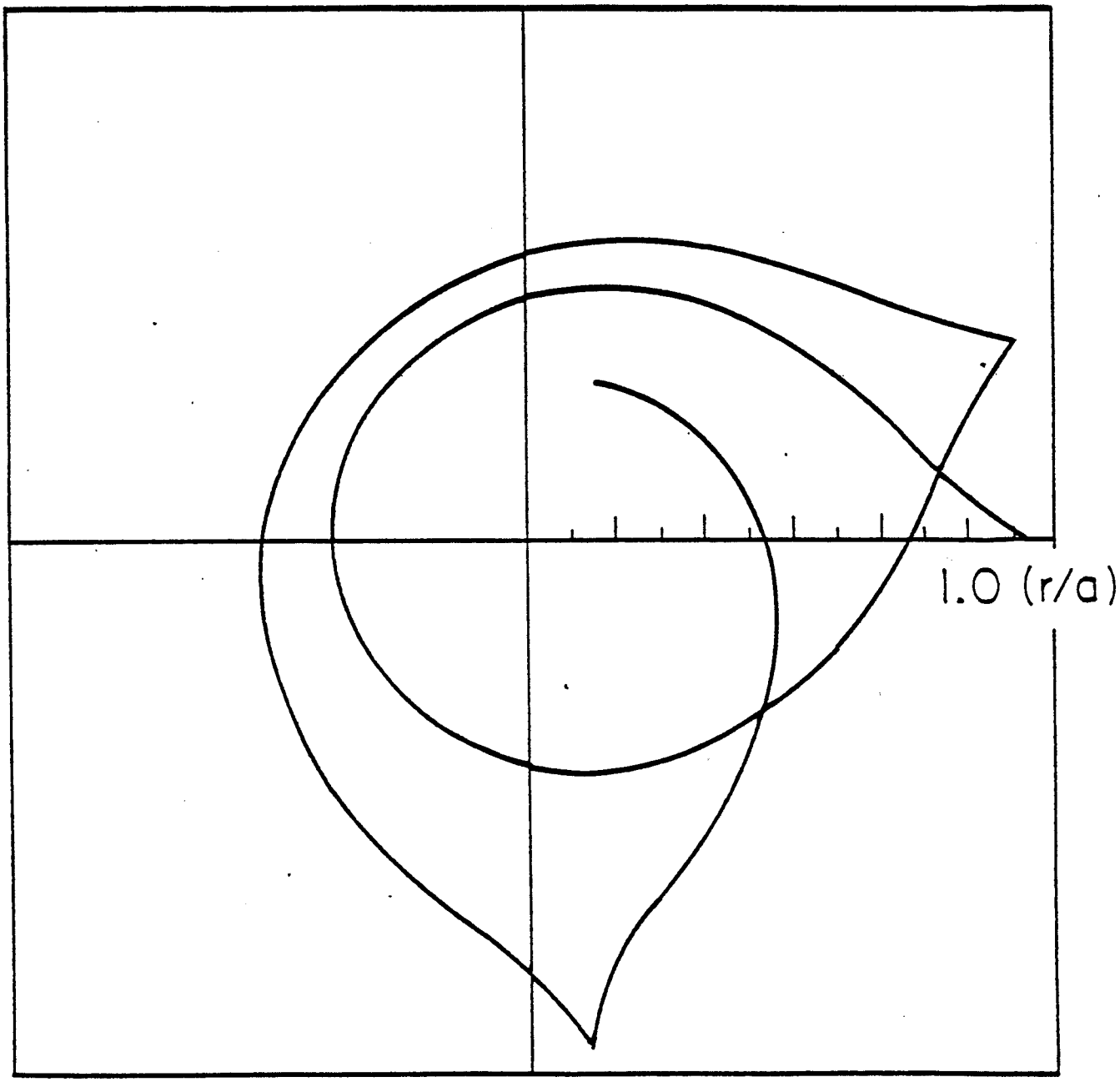

Figure 3(a).

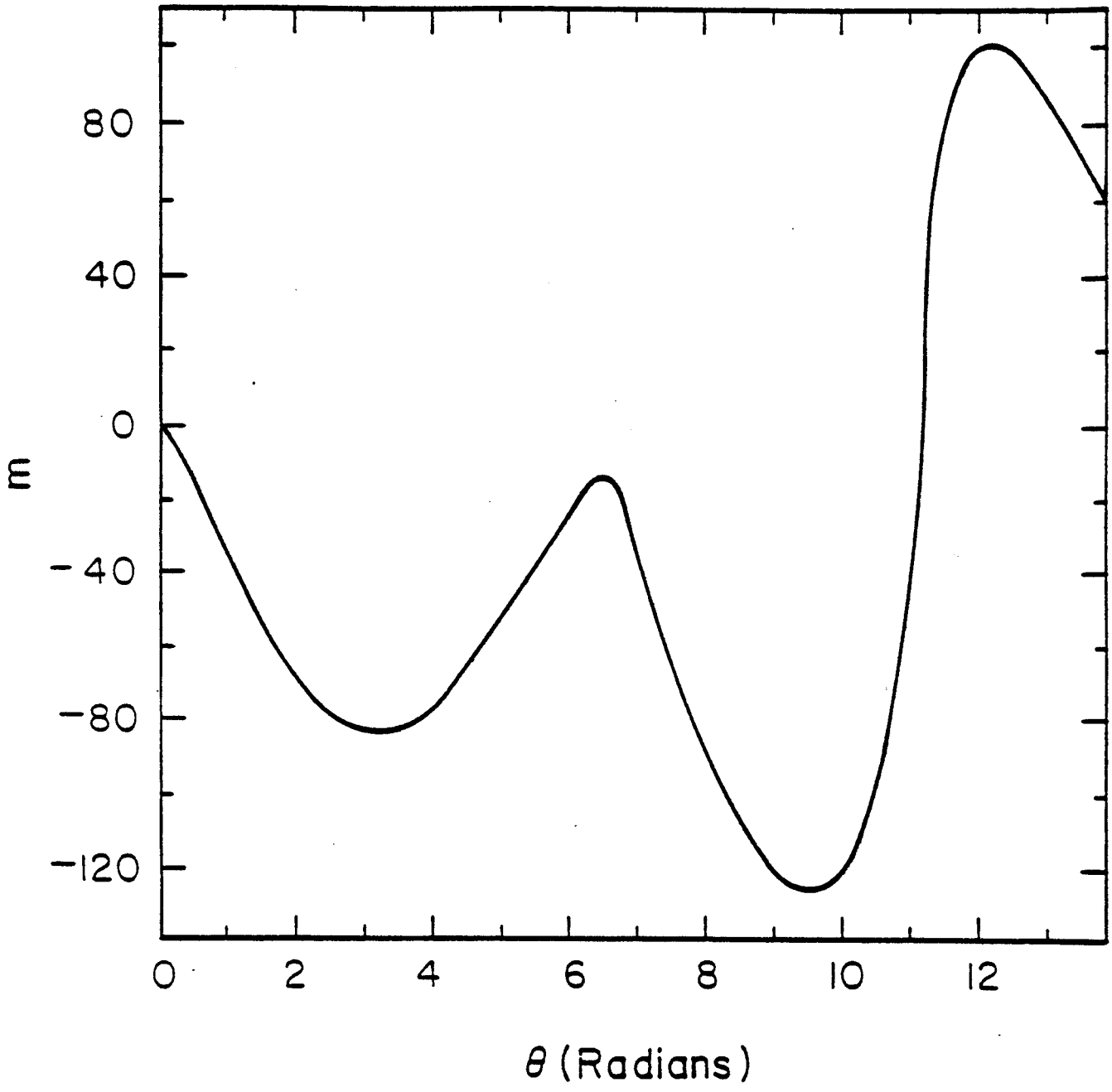

Figure 3(b).

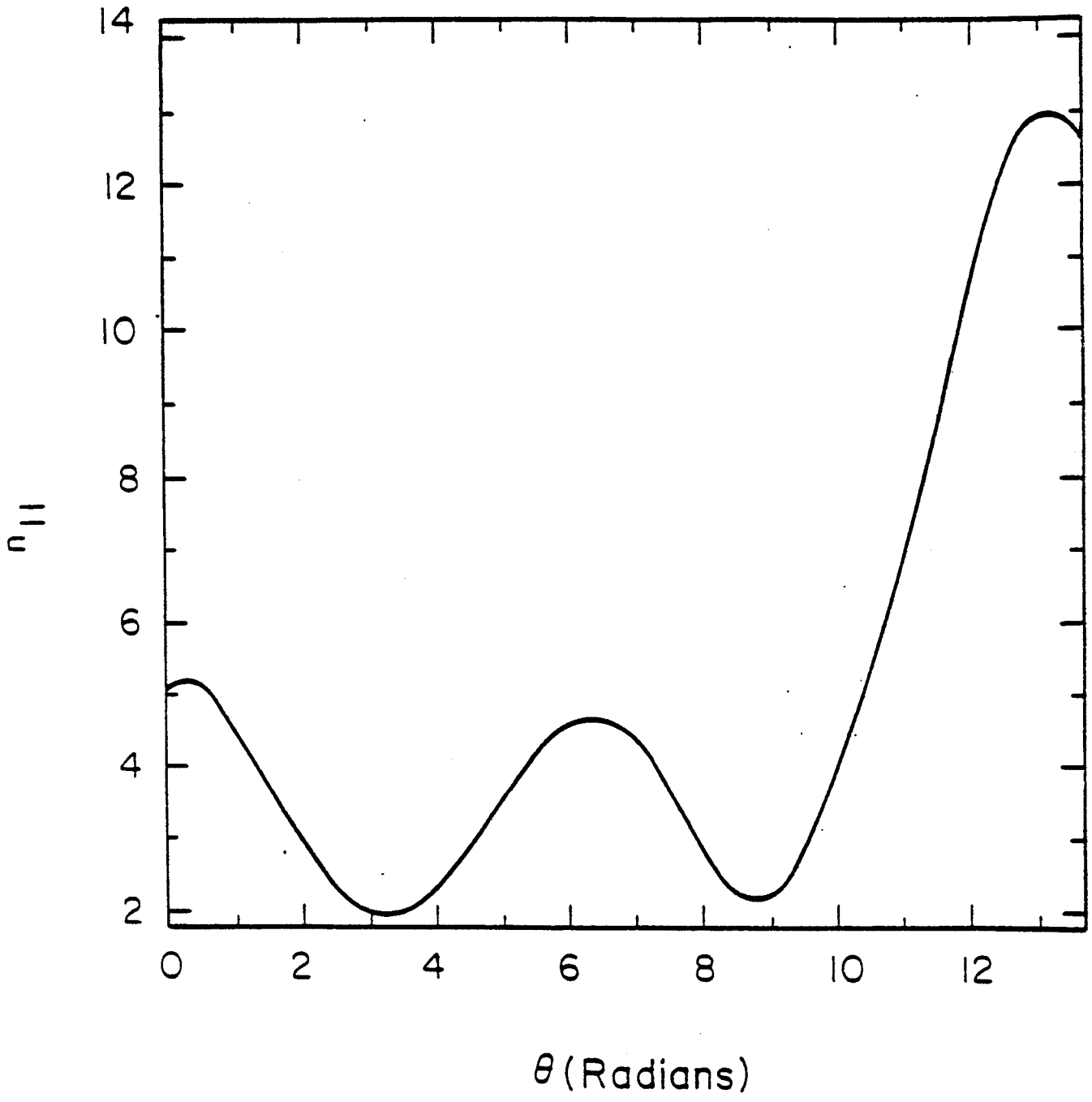

Figure 3(c).

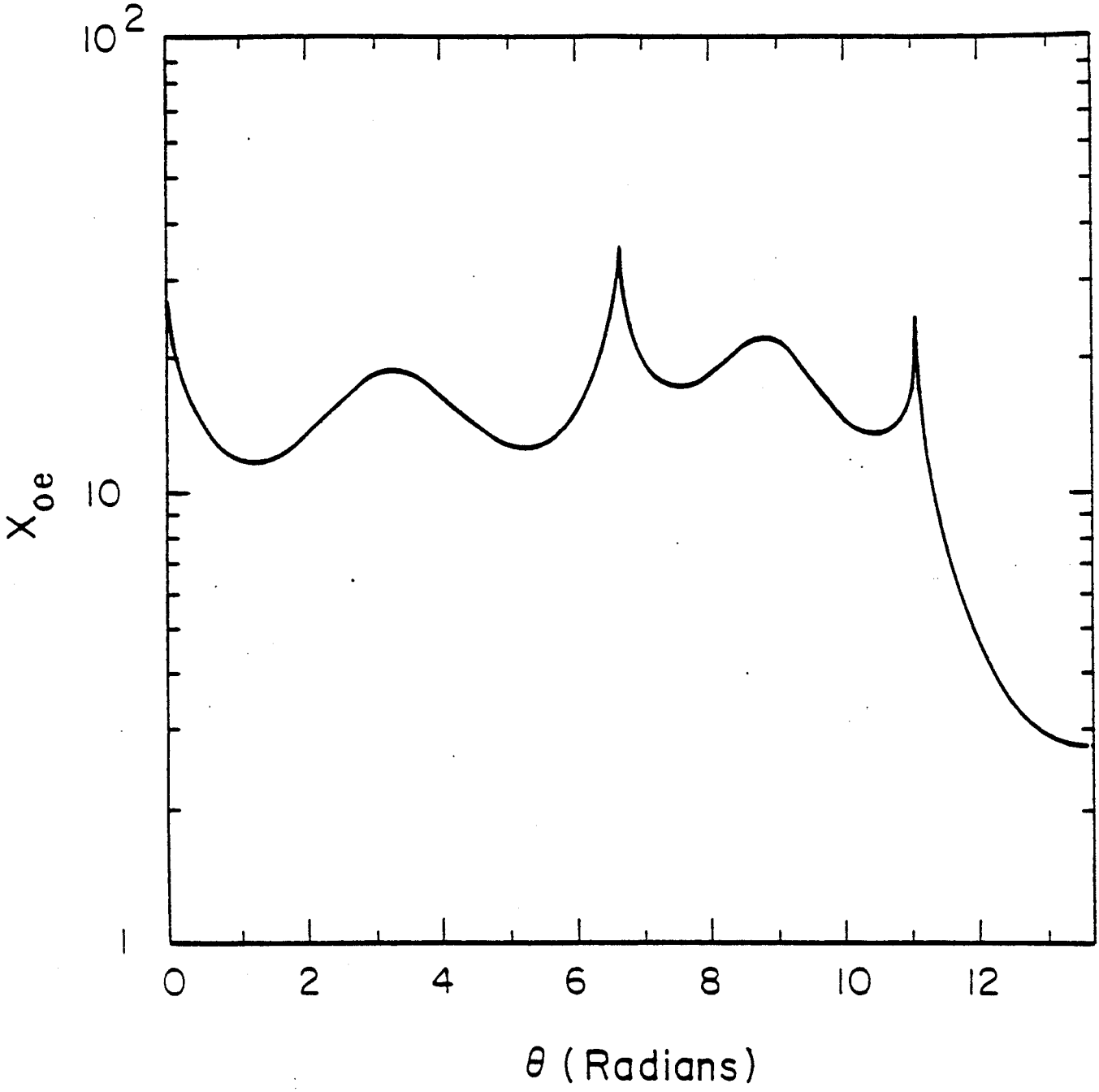

Figure 3(d).

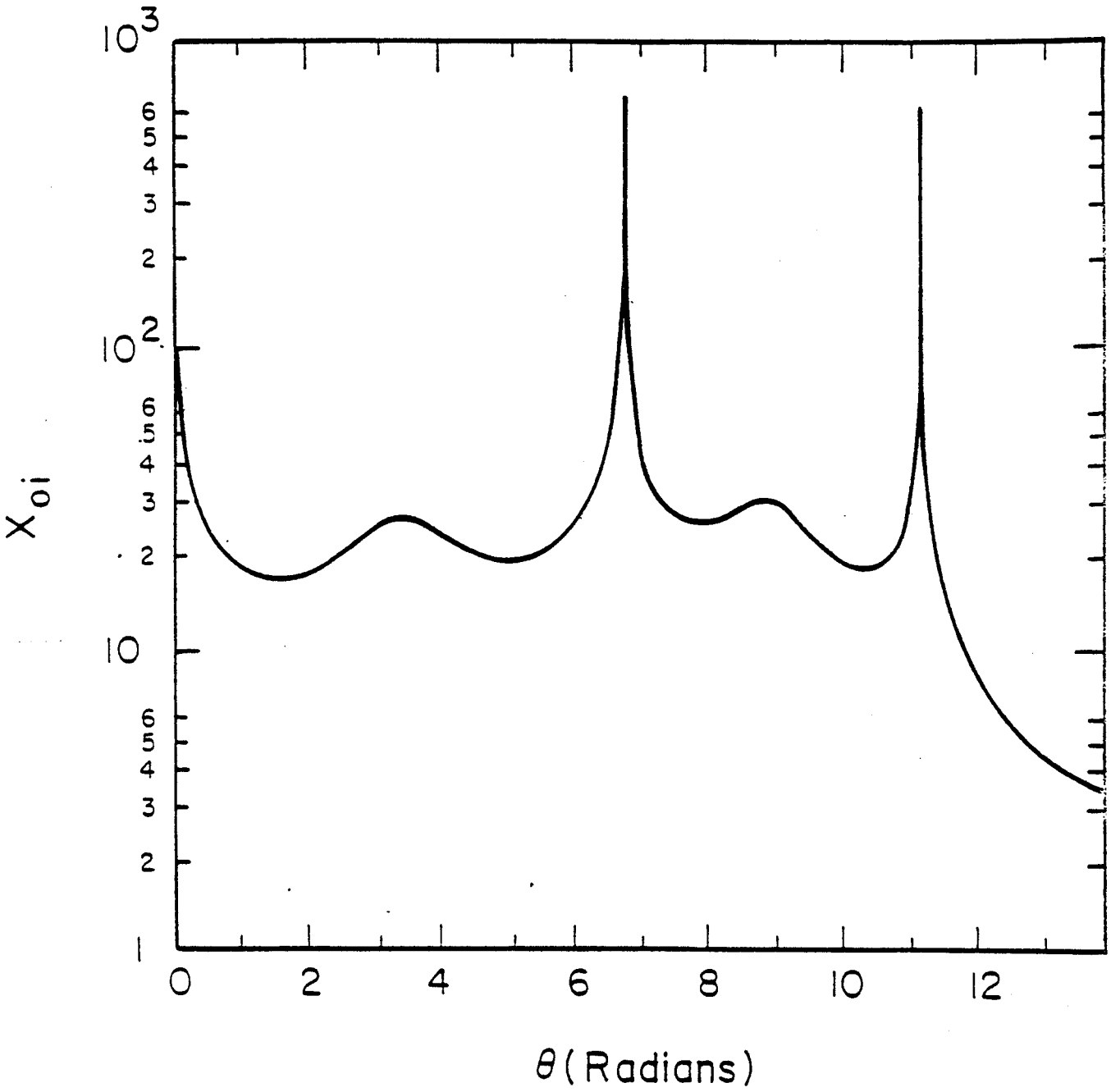

Figure 3(e).

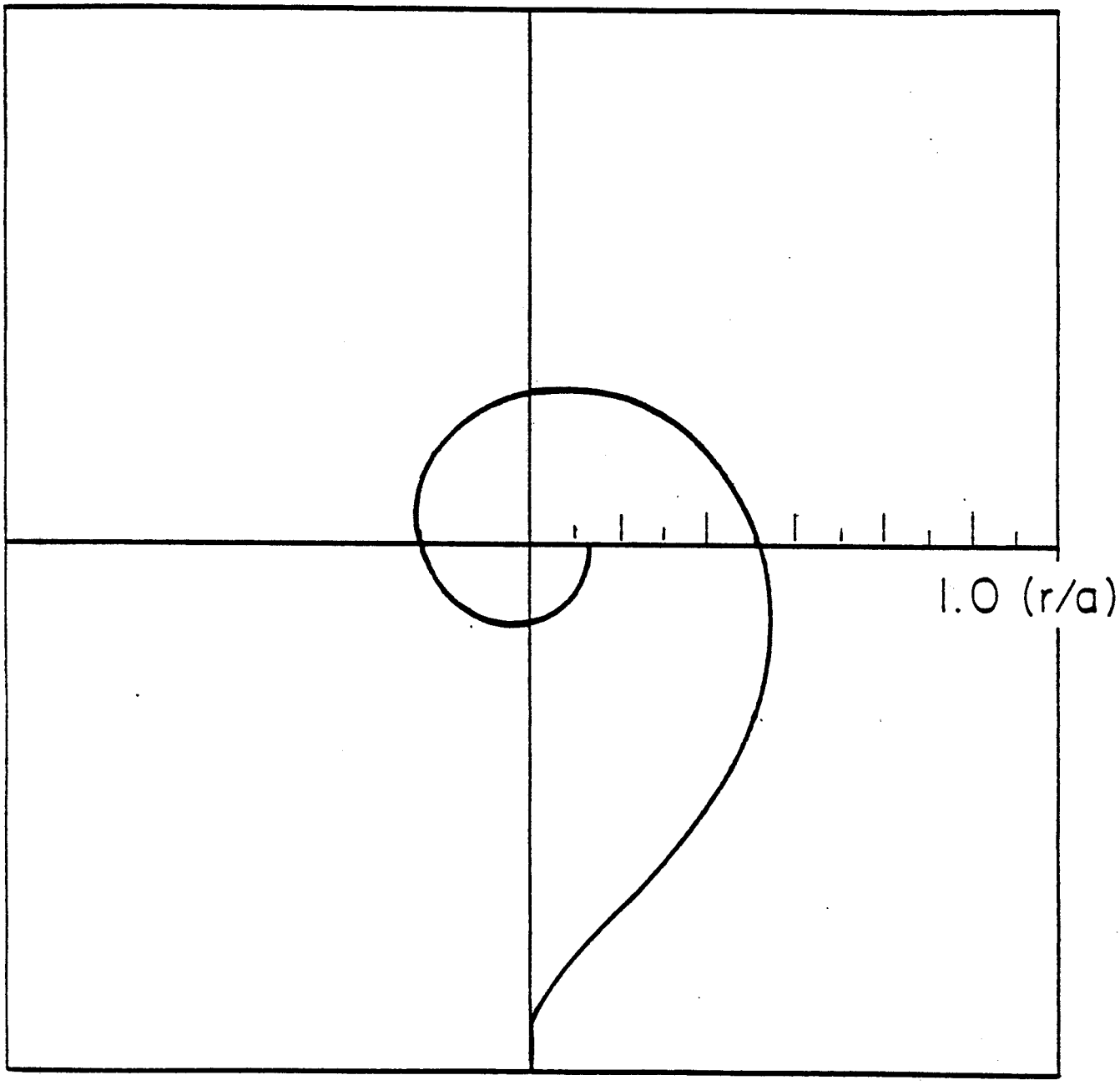

Figure 4(a).

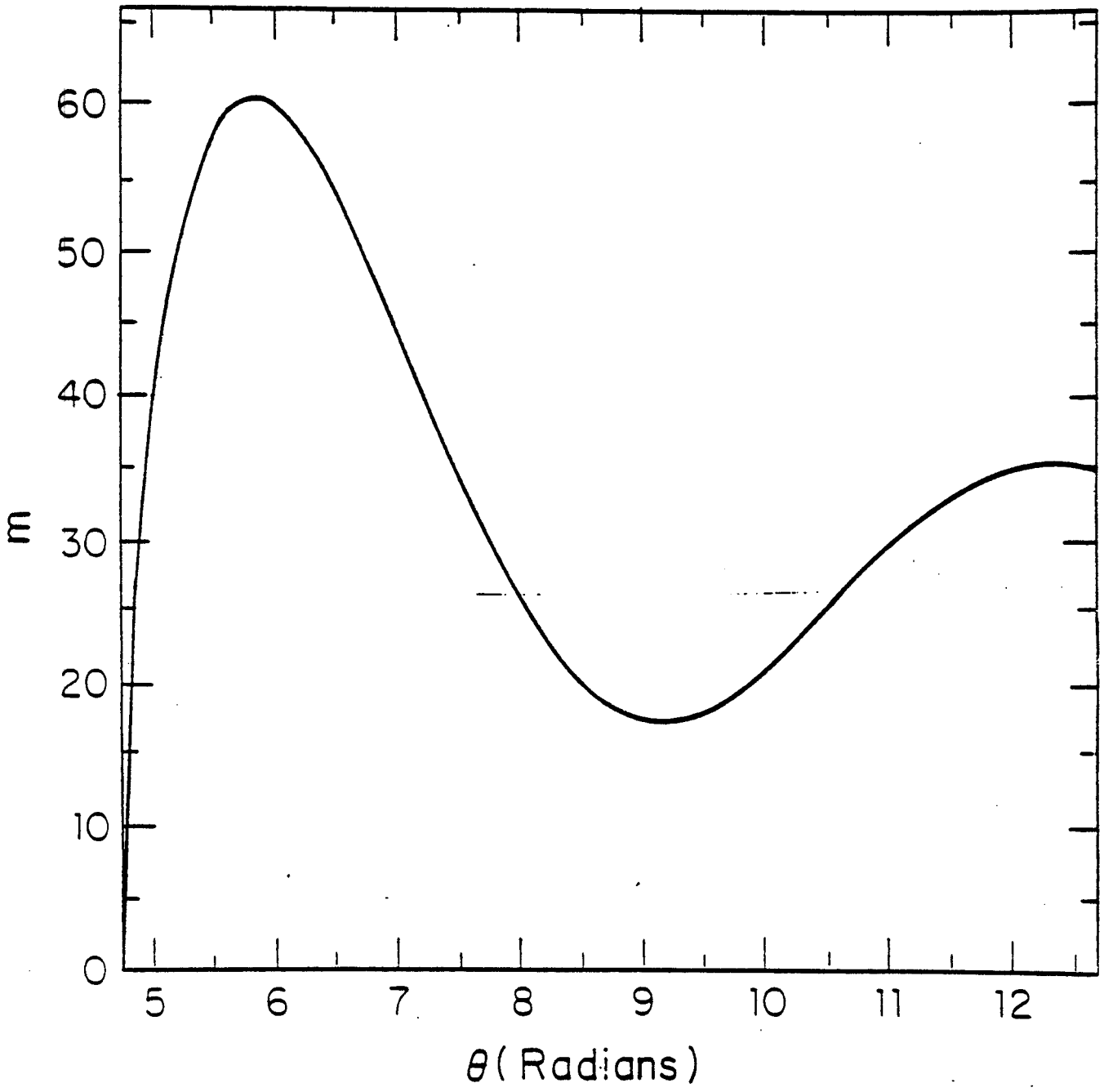

Figure 4(b).

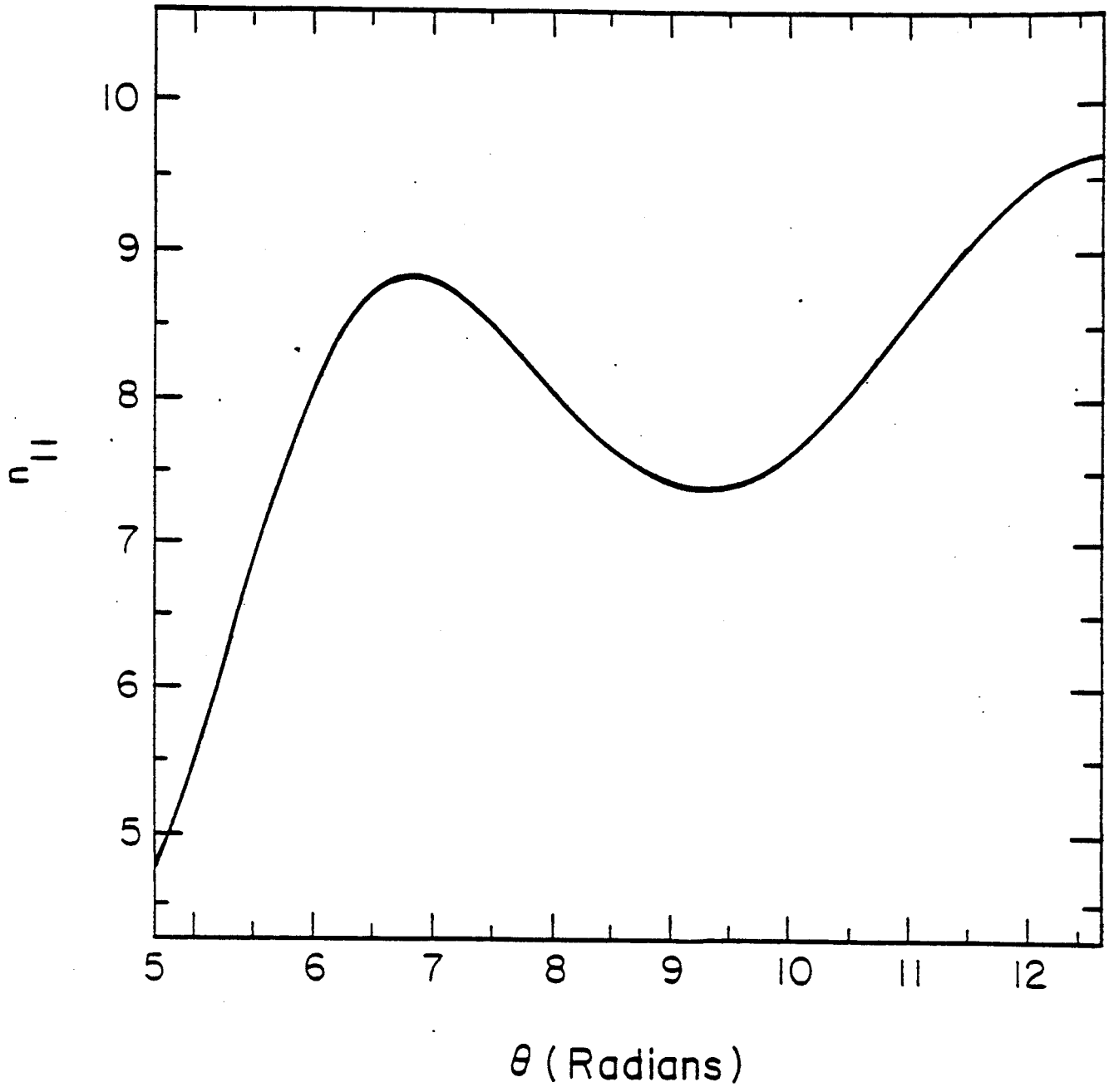

Figure 4(c).

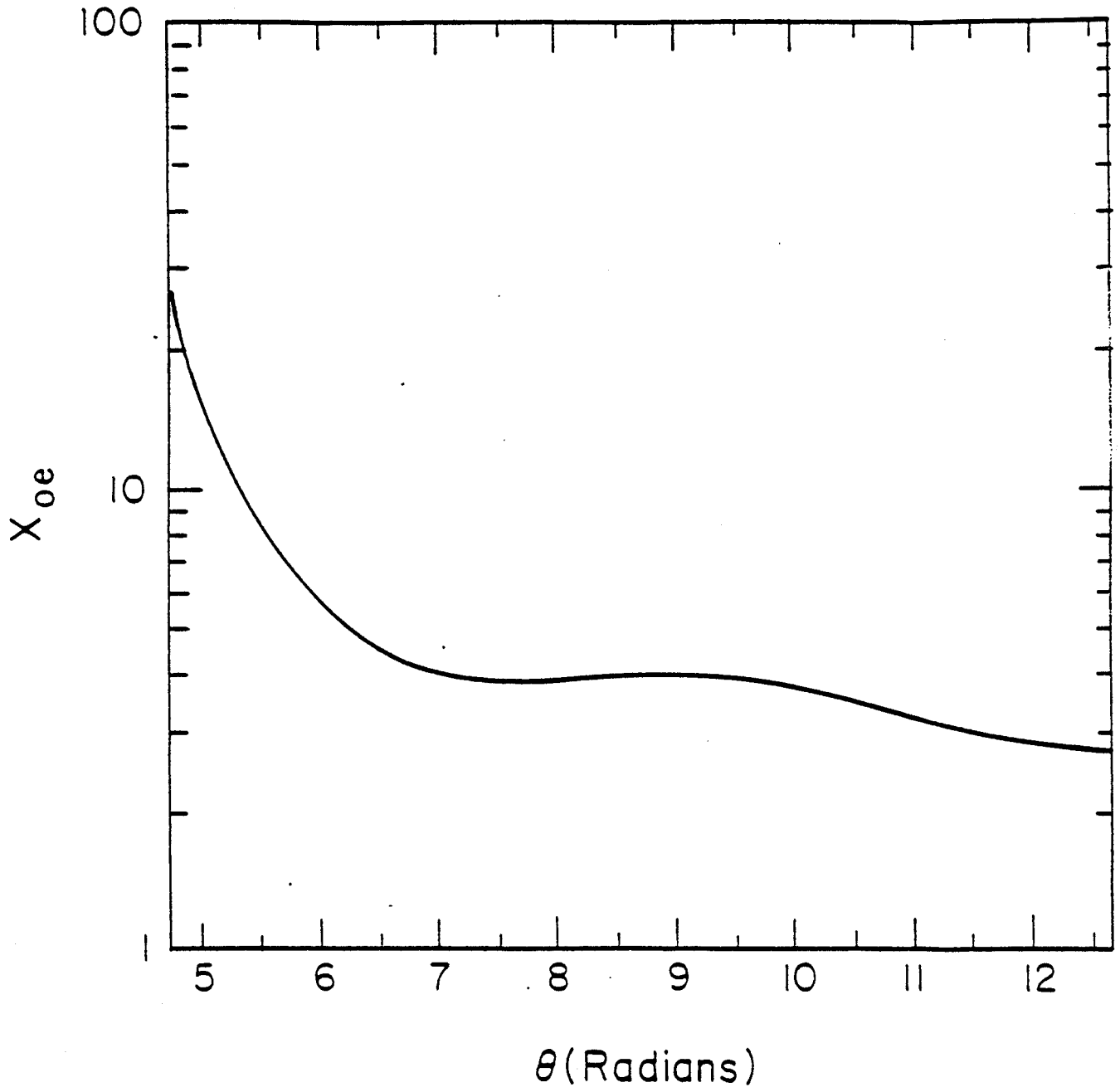

Figure 4(d).

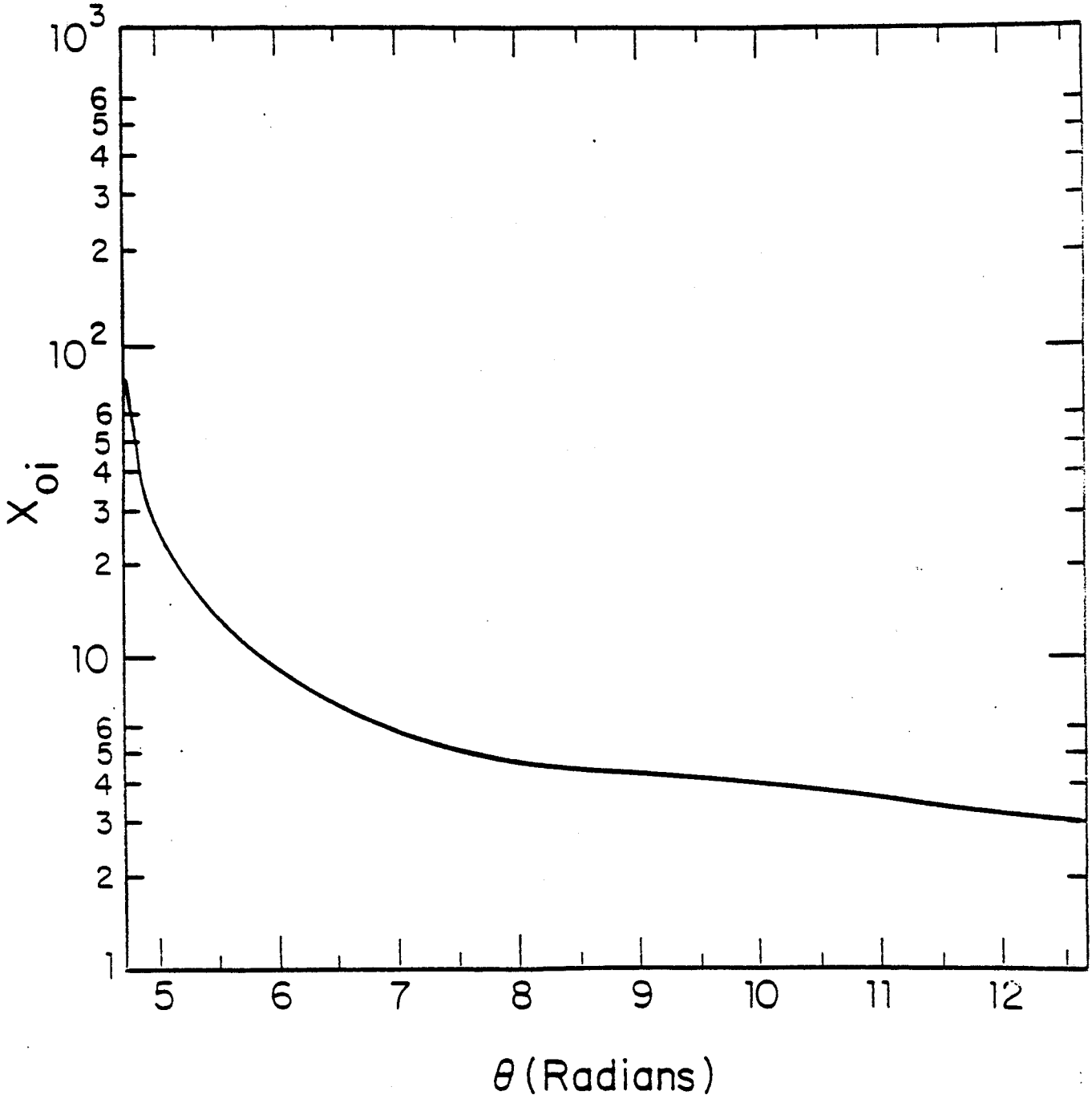

Figure 4(e).

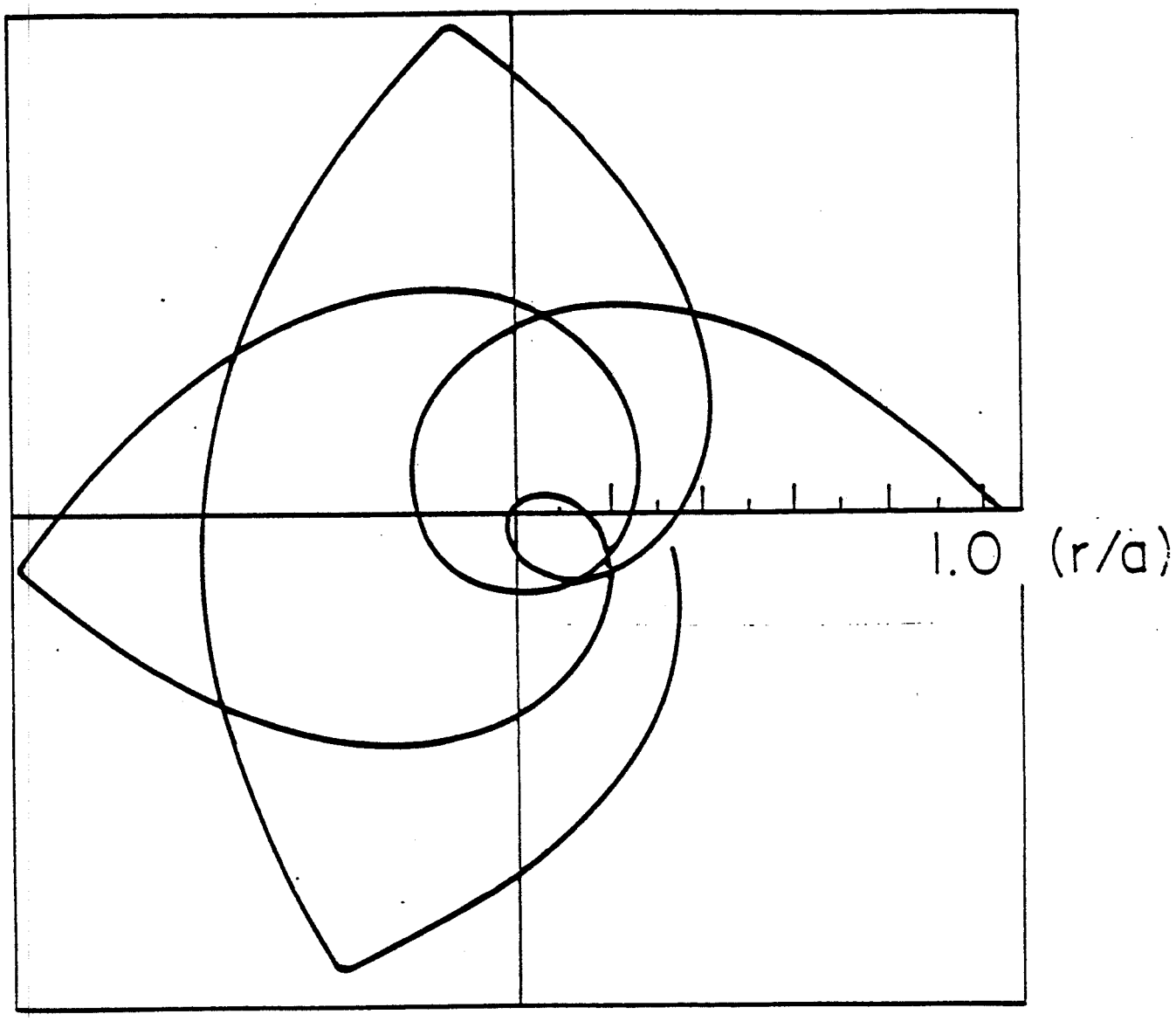

Figure 5(a).

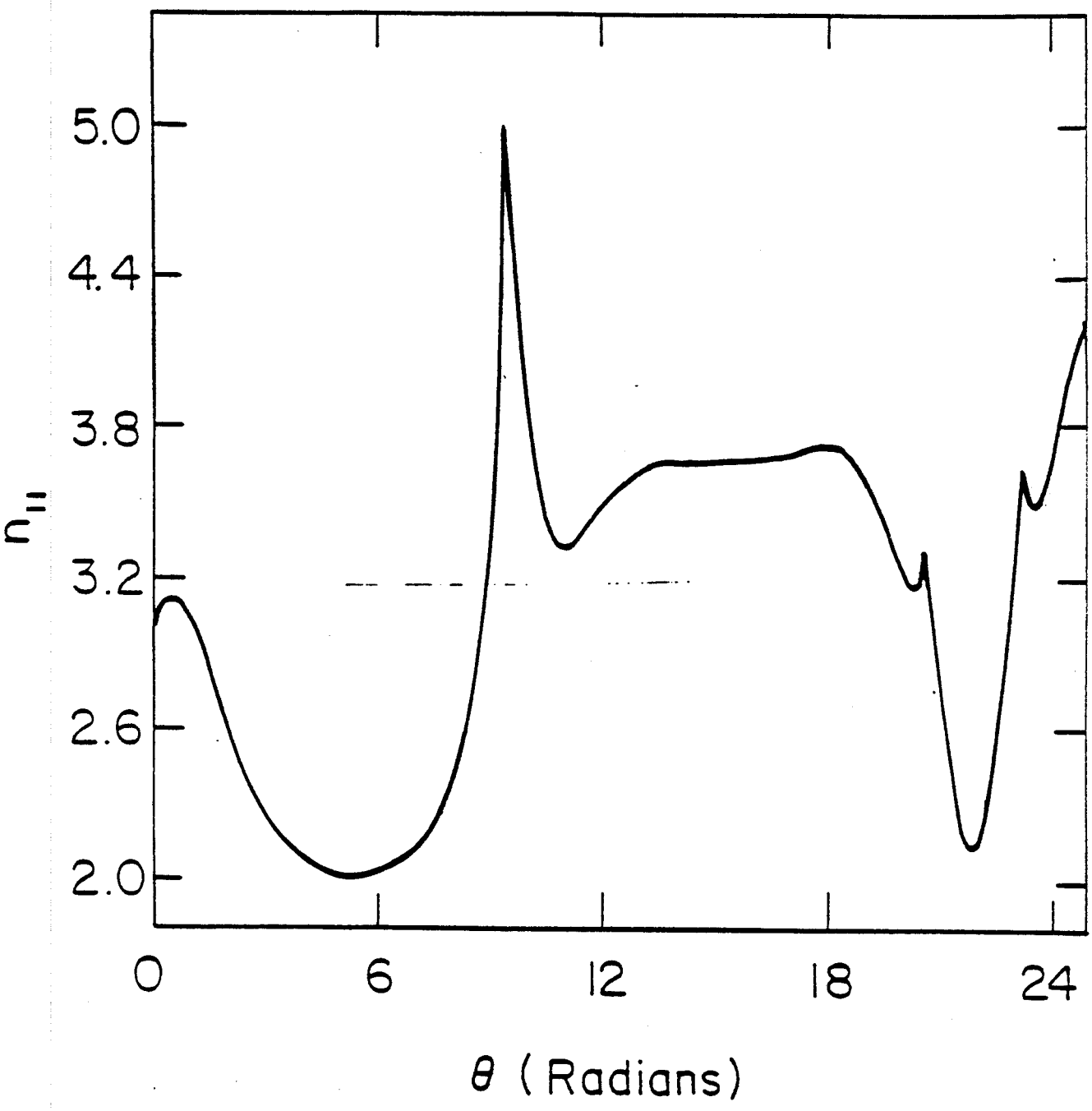

Figure 5(b).

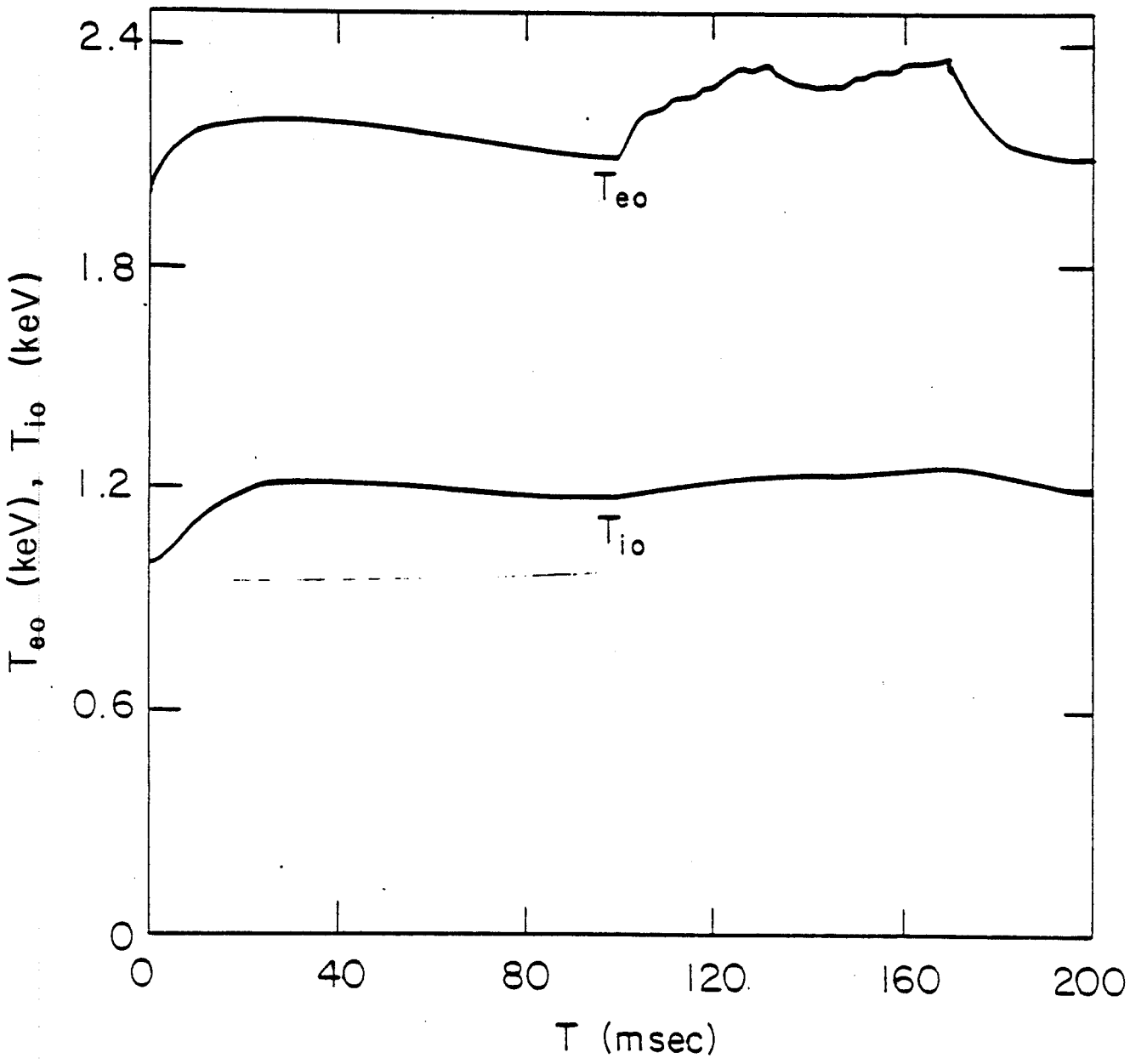

Figure 6(a).

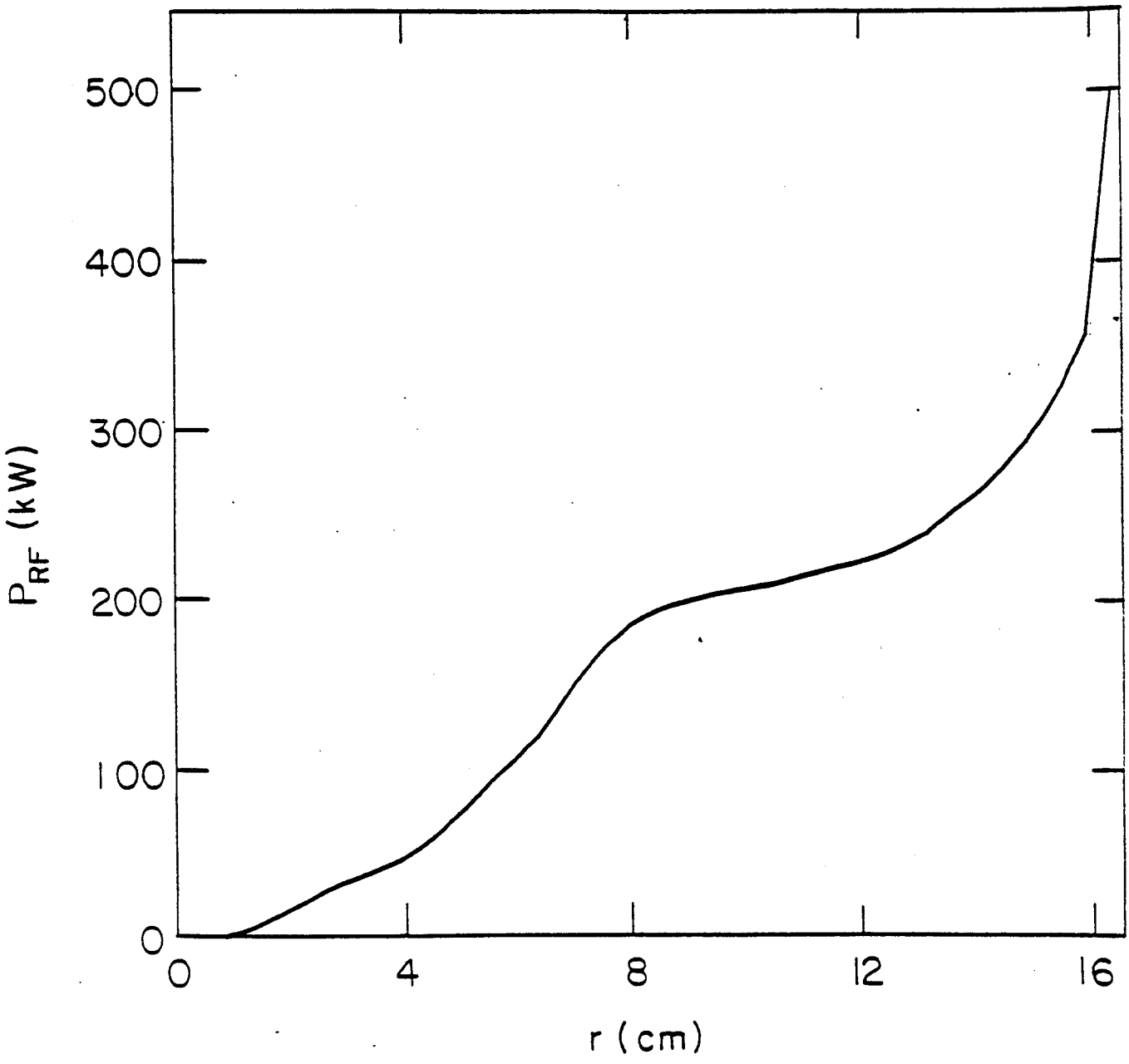

Figure 6(b).

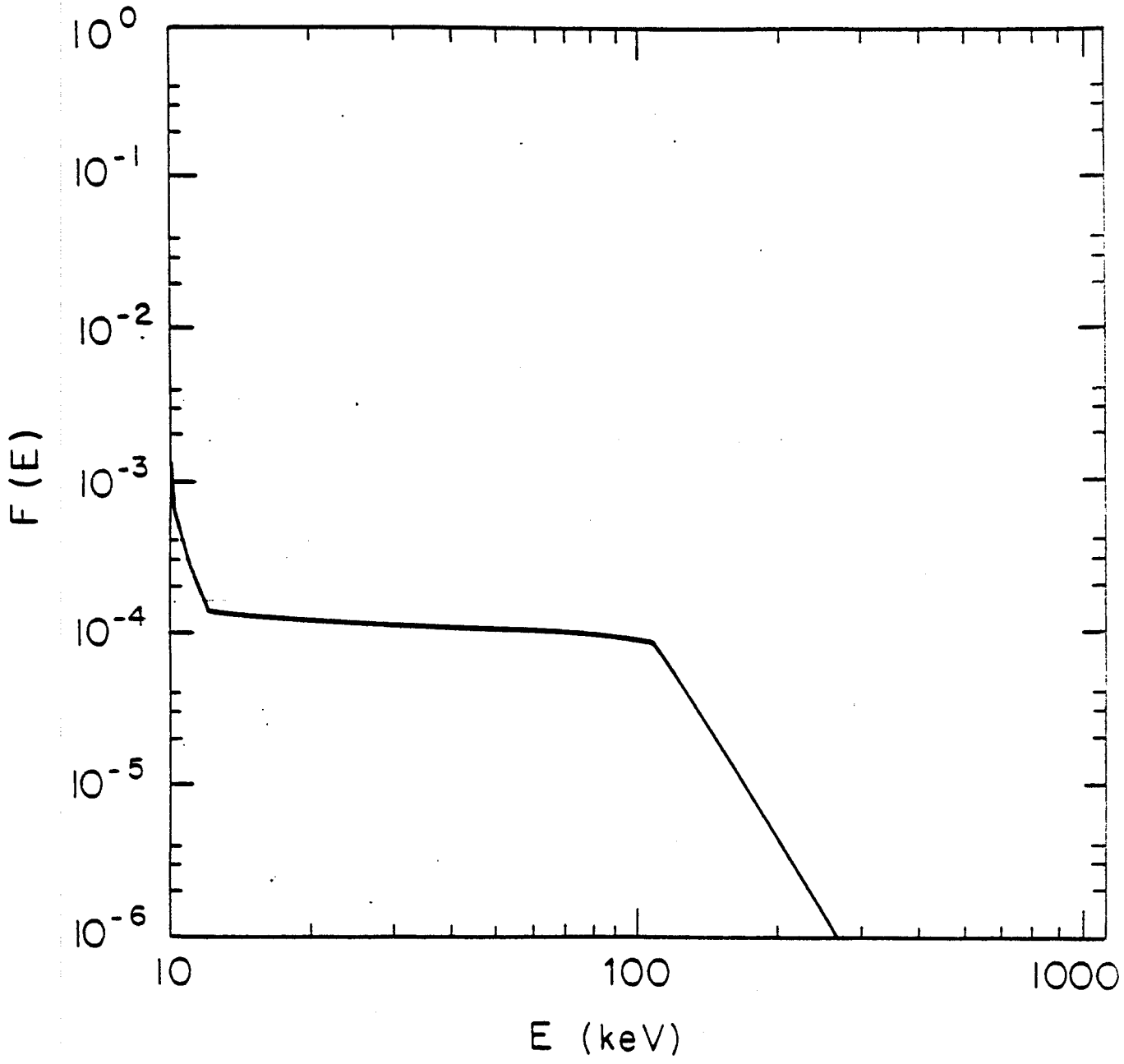

Figure 6(c).